PHOTOLUMINESCENCE SPECTROSCOPY OF POLYEXCITONS AND THERMALLY GENERATED DEFECTS IN Si

by

Alan G. Steele

B.Sc., University of Toronto, 1984

THESIS SUBMITTED IN PARTIAL FULFILLMENT OF

THE REQUIREMENTS FOR THE DEGREE OF

DOCTOR OF PHILOSOPHY

in the Department

of

Physics

SIMON FRASER UNIVERSITY

December 1988

APPROVAL

Name: Alan G. Steele

Degree: Ph.D. Physics

Title of Thesis: Photoluminescence Spectroscopy of Polyexcitons and Thermally Generated Defects in Si

Examining Committee:

Chairman: Dr. E.D. Crozier

Dr. M.L.W. Thewalt
Senior Supervisor

Dr. B.P. Clayman

Dr. G. Kirczenow

Dr. J.C. Irwin

Dr. T. Timusk
External Examiner
Department of Physics
McMaster University

Date Approved: December 19, 1988

PARTIAL COPYRIGHT LICENSE

I hereby grant to Simon Fraser University the right to lend my thesis, project or extended essay (the title of which is shown below) to users of the Simon Fraser University Library, and to make partial or single copies only for such users or in response to a request from the library of any other university, or other educational institution, on its own behalf or for one of its users. I further agree that permission for multiple copying of this work for scholarly purposes may be granted by me or the Dean of Graduate Studies. It is understood that copying or publication of this work for financial gain shall not be allowed without my written permission.

Title of Thesis/Project/Extended Essay

Photoluminescence Spectroscopy of Polyexcitons and Thermally Generated Defects in Silicon

Author: _____
(signature)

Alan George Steele
(name)

Dec 21/88
(date)

ABSTRACT

The analogy between excitons and positronium atoms has been useful in developing our understanding of solid state physics, and the existence of stable multi-electron-hole-pair species in semiconductors was postulated in 1958. Using photoluminescence near twice the band-gap energy, we made the first observation of free polyexcitons (n>2) in a semiconductor and obtained the molecular binding energies of triexcitons and tetraexcitons in Si.

Thermal annealing of oxygen-rich Si near 450°C produces a variety of defects, including the well-known thermal donors seen in infrared absorption. Photoluminescence spectroscopy has been used to identify these donors, and to study in detail two centres believed to be their remnant neutral cores. The two very similar isoelectronic centres are unique in that they can bind up to four excitons.

ACKNOWLEDGEMENT

Thanks are due to my senior supervisor, Mike Thewalt, for his encouragement, insight, and example in the laboratory. His ideas and criticisms were always on the button.

The generous financial support of the Natural Sciences and Engineering Research Council of Canada, the Advanced Systems Foundation of British Columbia, Simon Fraser University, and Dr. M.L.W. Thewalt is gratefully acknowledged.

Thanks to Linda for everything.

TABLE OF CONTENTS

TABLE OF CONTENTS (CONTINUED)

LIST OF TABLES

LIST OF FIGURES

LIST OF ABBREVIATIONS

BE	bound exciton
BMEC	bound multiexcitonic complex
CP	condensed plasma
Cz	Czochralski
DH	Dörnen and Hangleiter
e-h	electron - hole
EHD	electron hole droplet
FE	free exciton
FIR	far infrared
FZ	float zone
HTL	Hopfield, Thomas, and Lynch
IBE	isoelectronic bound exciton
IR	infrared
KFR	Kaiser, Frisch, and Reiss
LO	longitudinal optical
NP	no phonon
OPO	optical parametric oscillator
PE	polyexcitons
PL	photoluminescence
PLE	photoluminescence excitation
SW	Smith and Wolfe
TA	transverse accoustic
TD	thermal donor
TO	transverse optical
UHP	ultrahigh purity
WQ	Weber and Queisser

Chapter 1: Introduction to Excitons in Semiconductors

1.1: Free Excitons

An exciton is the elementary electronic excitation in semiconductors, and therefore is of fundamental importance in any discussion of their optical properties. There are two simple ways in which the exciton can be modelled, corresponding to different limits of the exciton size. The nature of the host crystal determines the exciton bohr radius (a_0), which in these convenient limits may be much smaller than the interatomic spacing (d), or very much larger.

In ionic materials, such as the alkali-halides, the excited electron remains tightly localized at the atom ($a_0 \ll d$), and the excitations are best described in terms of the atomic orbitals of the host: the electron is promoted to a higher energy orbital, leaving a hole behind in the unoccupied orbital. This type of intra-atomic exciton is known as the Frenkel exciton, and was first postulated in 1931. [31F]

In covalent materials such as the elemental semiconductor silicon which will be the subject of this thesis, the band picture [62L] provides a convenient description of the electronic states. The electron can be excited across the band gap into the conduction band, leaving a hole in the valence band. The electron and hole are free to move through the crystal, but interact via the Coulomb potential. These can be described as charged particles with effective masses m_e and m_h, respectively, which describe the

curvature of the relevant band extrema. [65K] The interaction potential:

$$V(\mathbf{r}_e - \mathbf{r}_h) = \frac{-e^2}{\varepsilon|\mathbf{r}_e - \mathbf{r}_h|} \qquad \ldots\ldots(1.1)$$

describes the interaction of an electron at $\mathbf{r}_e$ with a hole at $\mathbf{r}_h$ in a dielectric medium. In Equation 1.1, ε is the macroscopic dielectric constant of the crystal, which takes into account the effect of the polarizability of the host lattice. This description of the interaction will be valid when the orbital radius of the electron-hole relative motion is much larger than the interatomic distance ($a_0 \gg d$). The energy spectrum for the bound states of the exciton with internal potential given by Equation 1.1 can be written in direct analogy to the hydrogen atom as:

$$E_n = \frac{-\mu e^4}{2\hbar^2\varepsilon^2 n^2} \qquad (n = 1, 2, 3, \ldots) \qquad \ldots\ldots(1.2)$$

where μ is the reduced mass, $\mu = (m_e^{-1} + m_h^{-1})^{-1}$. Since the dielectric constant is quite large and the reduced mass is very small, the binding energy of free excitons (FE) will be of order 10 meV, and the excitonic Bohr radius will be of order 100 Å, thus justifying the use of the dielectric screening in the potential. These extended FE with $a_o \gg d$ are known as Wannier-Mott excitons, and were first proposed by Wannier in 1937. [37W]

A kinetic energy term must be added to the spectrum of bound levels given by Equation 1.2, since the excitons are free to move through the crystal, leading to a series of excitonic bands. The total mass of an

exciton is the sum of the electron and hole effective masses: $M = m_e + m_h$, and thus the total energy of an exciton in the state with principal quantum number n and translational wavevector **K** can be written as in Equation 1.3.

$$E_{nK} = \frac{-\mu e^4}{2\hbar^2 \varepsilon^2 n^2} + \frac{\hbar K^2}{2M} \qquad \ldots\ldots (1.3)$$

The discussion so far has implicitly assumed (by the simple choices of m_e and m_h) non-degenerate and parabolic band extrema located at the same point in *k*-space. For indirect gap semiconductors like Si, however, the situation is not so simple, and the inclusion of the more complicated band structure necessarily complicates the theoretical description of FE. [77L] The valence band maximum in Si is located at the Brillouin zone center (**k**=0) and is doubly degenerate (excluding spin). There are six equivalent conduction band minima located along the <100> directions 85% of the way to the zone boundary. These minima are ellipsoids of revolution, and thus two different effective masses (longitudinal mass $m_{el} = 0.9163$ and transverse mass $m_{et} = 0.1905$, in units of the free electron mass, m_0) are needed to describe the anisotropy. [65H]

The excited state series of indirect FE in Si has been studied experimentally using optical absorption in the far infrared (FIR) [78Tb] and the theoretical description of Lipari and Altarelli [77L] was considered to be in excellent agreement with these results. More recent high resolution FIR absorption spectra [88L] suggest that a new theoretical approach must be undertaken, however, and it is clear that the study of

this fundamental problem in semiconductors is still an area of active research.

Free excitons are also observed in photoluminescence (PL) studies of Si, where excitation with above band gap energy photons is used to create the FE gas. The initial hot electron and hole distributions cool very quickly by emitting phonons, and it is possible to regard the gas as being in thermal equilibrium with the lattice, on the timescale of FE recombination. The direct recombination of the electron (with $\mathbf{k}_e \cong 0.85 \cdot \mathbf{K}_0$) and hole (with $\mathbf{k}_h \cong \mathbf{0}$) is forbidden in indirect band gap semiconductors since momentum would not be conserved. By simultaneously emitting a phonon, however, momentum can be conserved and the decay of FE observed in the near infrared, shifted down from the Si band gap energy by the phonon energy and the exciton binding energy. The principal momentum-conserving phonons in Si [70S,77V] are the transverse acoustic (TA) with energy 18.4 ± 0.2 meV, and the longitudinal and transverse optical (LO = 56.2 ± 1 meV and TO = 58.0 ± 1 meV, respectively) phonons.

Since the FE binding energy in Si is only 14.7 meV [77L,70S], experiments must be conducted at cryogenic temperatures, as discussed in Chapter 2. The luminescence line shape of FE is well described by a Maxwell-Boltzmann distribution, which reflects the thermal kinetic energy distribution of the exciton gas, multiplied by a square-root density of states term. (This description of course neglects the effects of the electron-hole interaction, which splits the free exciton transition, and which leads to non-parabolicities in the exciton dispersion within a few tenths of an meV from the conduction band minimum.) The observed lifetime of FE in pure Si is quite long, typically being in the range of 0.5 to 50

μs at 2 to 15 K [80H]. The presence of impurities which can quickly trap the FE will decrease the observed lifetime since this parallel non-radiative process also decreases the FE population. [80H]

1.2: Larger Excitonic Complexes: Biexcitons and Polyexcitons

At higher densities of the exciton gas, the question of exciton interactions arises, and the possibility of larger stable excitonic species must be considered. In 1958, Lampert [58L] first postulated the existence of such complexes arguing in analogy with hydrogenic or positronium systems. He proposed a number of new excitonic species, including donor- and acceptor-bound excitons (both neutral and charged), trions (free complexes of two holes and one electron, or *vice versa*), overcharged donors and acceptors (D^- and A^+, respectively), and finally, the (free) excitonic molecule or biexciton.

The first observation of biexcitons in an indirect gap semiconductor was in AgBr [76P,77Hc], and Thewalt and Rostworowski [77T] presented the first observation of the PL of biexcitons in Si. They [77T] fit the Biexciton -> photon + TA_{phonon} + 1s-exciton luminescence line shape using the model of Cho [73C] at two temperatures, and obtained a biexciton molecular binding energy of 1.2 meV. This value was later refined by Thewalt and McMullan [84T] who observed the complete annihilation of stationary biexcitons via the green PL signal detected near twice the Si band gap energy: they obtained a biexciton binding energy relative to the lowest energy FE edge of 1.36 ± 0.26 meV.

Although Brinkman and Rice [73B] have shown that in simple non-degenerate parabolic band structures no stable complexes larger than the biexciton can exist, the extra band-edge degeneracy in Si (and Ge) can dramatically affect the stability calculations. Wang and Kittel [72W]

first pointed out that more than two electrons could be placed in the lowest energy orbital in these materials without violating the Pauli exclusion principle. Morgan [77Mb] later considered the stability of these large neutral species in Si, and concluded that complexes containing up to six electron-hole (*e-h*) pairs would be stable. The first experimental observation of these large free excitonic complexes, referred to as polyexcitons (PE), was reported by Steele *et al.* [87Sa], who observed the green PL from complexes containing up to five *e-h* pairs, and deduced molecular binding energies of 3.83 and 6.34 meV for triexcitons and tetraexcitons, respectively, in ultrahigh purity Si. These experiments and results are the subject of Chapter 6 of this thesis.

1.3: The Electron-Hole Droplet

The electron-hole droplet (EHD) was first observed by Haynes in the PL spectrum of high-purity Si at lower energy than the NIR FE recombination discussed above, but was incorrectly attributed at this time to biexciton recombination. [66Ha] It was Keldysh [68K] who first proposed that the PL results of Haynes [66Ha] and the photoconductivity results of Asnin and Rogachev [68A] could be explained in terms of a high density metallic liquid composed of electrons and holes. The EHD was the subject of review articles by Rice [77R], on the theoretical approach and background, and by Hensel *et al.* [77Hb], on the experimental aspects, and the reader is referred to these sources for more detailed information and many further references.

The luminescence line shape of EHD recombination [77R] is obtained from the convolution integral over the electron and hole density of states functions multiplied by the appropriately altered Fermi distributions which account for the presence of the liquid. The phonon-assisted luminescence features associated with EHD recombination have line shapes given by:

$$I(h\nu) \propto \int_0^\infty d\varepsilon_e \int_0^\infty d\varepsilon_h \, D_e(\varepsilon_e) \, D_h(\varepsilon_h) \, f_e(\varepsilon_e) \, f_h(\varepsilon_h) \times \delta(\varepsilon_e + \varepsilon_h + E_{gap} - h\nu - \hbar\omega_{ph}) \qquad \ldots\ldots (1.4)$$

where E_{gap} is the energy gap, $D_{e,h}$ are the densities of states, and $f_{e,h}$ are the Fermi functions. The energy of the momentum-conserving phonon is

$\hbar\omega_{ph}$. The luminescence line shape obtained from this function is asymmetric, with a sharp, linear drop to zero at the high energy side (from which a spectroscopic measure of the binding energy of the droplet may be obtained) and a quadratic tail to low energy. From the width of the line, $E_{Fe} + E_{Fh}$ is calculated inside the drop. As pointed out by Rice [77R], even this simple model gives a remarkably good fit to the experimentally observed luminescence line shape, although additional corrections such as the lifetime broadening of the final states of radiative transitions calculated by Martin and Störmer [77Ma] must be made in order to fit accurately the observed low energy broadening. [79S]

Schmid [76S,79S] has reported the thermodynamical parameters of the EHD in Si. At a carrier temperature of 5 K, the *e-h* pair density was $n = 3.5 \times 10^{18}$ cm^{-3}, the work function $\Phi = -9.3$ meV, and the intrinsic recombination lifetime was $\tau = 140$ ns. Gourley and Wolfe [81G,82G] obtained similar results and further considered the high-stress limit of the EHD. They determined the critical temperature for the gas - liquid phase transition to be $T \cong 20$ K, and the critical density to be $n_c \cong 2.5 \times 10^{17}$ cm^{-3}. Gourley and Wolfe [81G] also summarize the results of other workers and list more recent references than are found in Rice. [77R]

1.4: Bound Excitons

As predicted by Lampert [58L], excitons can become bound at impurities in the crystal, further decreasing their energy by the exciton localization energy at the defect. The first experimental observation of donor and acceptor bound excitons (BE) was made by Haynes [60H], using PL to investigate Si selectively doped with several different group V donors and group III acceptors. The BE transitions were observed as very narrow lines in PL, since the recombining particles are localized at the impurity and therefore do not have the Maxwell-Boltzmann distribution of kinetic energy which characterizes the FE luminescence line shape. The spectral position of BE transitions in Si, from which the exciton localization energy may be obtained directly, depends on the nature of the impurity center. This is not predicted by simple effective mass theory, in which all BE have the same binding energy, and is accounted for by what has become known as the "central cell" correction. [73D, 76B]

The impurity-specific central cell potential, which must be added to the Coulomb interaction for donor and acceptor BE, is responsible for the differences in exciton localization energy. This was treated by Dean [73D] and Baldereschi and Lipari [76B] as a first-order correction to the effective mass result. They introduced the central cell potential, V_c, which adds a linear energy correction to the effective mass impurity binding energy, $(E_i)_{EM}$, and to the effective mass exciton localization energy, $(E_{BX})_{EM}$. This additional potential accounts for the effects of the impurity atom in the host crystal, including the difference in atomic

potentials and any strain field associated with the defect. The total binding energies may be written as:

$$E_1 = (E_1)_{EM} + V_c \rho_c \qquad \ldots\ldots (1.5)$$

$$E_{BX} = (E_{BX})_{EM} + V_c \delta\rho_c \qquad \ldots\ldots (1.6)$$

where ρ_c is the average electronic charge density in the central cell region for the neutral impurity state, and $\delta\rho_c$ is the additional charge due to the localized exciton.

The exciton localization energy is given by the difference between the BE transition energy and the zero-kinetic-energy FE transition energy. Haynes [60H] plotted the localization energies of both donor and acceptor BE as a function of the ionization energy of the impurity involved, and observed a linear dependence. This empirical rule is known generally as Haynes' Rule, and may be expressed as follows.

$$E_{BX} = a \cdot E_1 + b \qquad \ldots\ldots (1.7)$$

The constants a and b in Equation 1.7 are material dependent, and for Si, $a \cong 0.1$, and $b = 0$. [60H]

Equations 1.5 and 1.6, which give the effective mass localization energy corrected for the presence of the central cell potential may be combined and put in the form of Haynes' Rule (Equation 1.7) as:

$$E_{BX} = \frac{\delta\rho_c}{\rho_c} E_1 + \left[(E_{BX})_{EM} - (E_1)_{EM} \frac{\delta\rho_c}{\rho_c} \right] \qquad \ldots\ldots (1.8)$$

and now the constants a and b in Equation 1.7 may be identified as

follows. [73D]

$$a = \frac{\delta\rho_c}{\rho_c} \qquad \ldots\ldots(1.9)$$

$$b = \left[(E_{BX})_{EM} - (E_i)_{EM} \frac{\delta\rho_c}{\rho_c} \right] \qquad \ldots\ldots(1.10)$$

In addition to observing different localization energies for the different BE species, Haynes also found that the intensity of the BE PL relative to the FE signal was proportional to the concentration of the impurity in the sample, when low excitation power densities are used to avoid saturating the bound excitons. [60H] This fact suggests that PL spectroscopy can be used as a method of characterizing Si samples, giving not only the chemical nature of the impurity species, but their absolute concentrations. The development and application of this characterization technique has been pursued by a variety of authors, led by Tajima [78Ta] in 1978, and recently calibration factors for B, P, and Al in Si in the range 10^{12} to 10^{15} cm^{-3} have been published by McL Colley and Lightowlers [87Ma].

It is also possible for neutral defects, the so-called isoelectronic centers, to localize excitons through the different atomic potential or a local strain field in the vicinity of the defect, thus creating an attractive potential for either electrons or holes, or possibly for both. Many such isoelectronic bound exciton (IBE) systems have been observed in PL of Si (see, e.g. [84W] and references therein) since the first observation in 1979 [79Wa], although most are not well characterized due to their complexity: none of these isoelectronic centers which can bind

excitons in Si is a point defect - but rather are atomic pairs or larger complexes.

The theoretical treatment of isoelectronic centers which are attractive to only one particle (either the electron or the hole) was given by Hopfield, Thomas, and Lynch (HTL).[66Hb] Once an electron (hole) is localized by the isoelectronic center, the defect becomes charged, and has a long-range Coulomb field which can bind a hole (electron). By separating the potentials which bind each particle, the HTL model is able to predict the excited state structure of the IBE, which are then classified as either donor-like (hole attractive defects) or acceptor-like (electron attractive defects). There are examples of both types of IBE in Si, as revealed by far infrared absorption studies of the BE excited states: the Be-related isoelectronic center has acceptor-like excited states [85Ta] while the recently-discovered sulphur-related S_A and S_B centers have donor-like excited states.[88T] Isoelectronic centers with axial symmetry have also been treated using an extension of the HTL model which incorporates an internal uniaxial strain along the defect axis, as described in the review article by Davies.[84D]

Another type of isoelectronic center is one in which *both* the electron and the hole are tightly localized by the defect. for these systems, the HTL model cannot describe the electronic states of the IBE since analogies with the hydrogen atom are no longer appropriate, and no detailed theoretical description for these centers exists.[71A] On the other hand, it is possible for both the electron and the hole to be only loosely bound, via an extended strain well potential for example. The binding mechanism of the isoelectronic O- and O'-centers [86T,87Sb], which are the subject of

Chapters 4 and 5 of this thesis, has not been characterized.

Several review articles concerning BE have been written, including the extensive treatment by Dean and Herbert [73D], the recent review of isoelectronic centers by Monemar [87Mb], and the exhaustive study of PL systems in Si by Davies [88D], which lists over 100 observed luminescence centers, emphasizing carbon-related and damage-induced defects.

1.5: Bound Multiexcitonic Complexes

Just as it is possible for a single *e-h* pair to become localized at an impurity site, forming a BE, in many cases more than one such pair can become localized at the same defect, and the resulting system is known generally as a bound multiexcitonic complex (BMEC). When an electron and a hole within such a complex recombine, the luminescence is observed as one of a series of sharp lines lying at energies below the principal BE transition associated with the same impurity center. These PL line series, and the first proposed BMEC explanation, were first published by Kaminskii and Pokrovskii [70K], although no detailed theoretical model had been formed, nor had the existence of such complexes been predicted in advance.

The history and a detailed description of the PL spectroscopy of BMECs in Si has been reviewed by Thewalt. [82T] A complete description of the observed BMEC transitions for several different centers was made possible by the shell model of Kirczenow [77Ka, 77Kb] which describes the wavefunction of the complex in terms of the properly antisymmetrized single particle wavefunctions, classified according the their group theoretical transformation properties under the tetrahedral point group T_d. This model was able to explain all of the observed major transitions and their behaviour under external perturbations such as a uniaxial stress or magnetic field, though it of course does not deal with the fine structure arising from e-e, e-h, or h-h interactions within the complex.

Although the details of the theory are beyond the scope of this thesis, a brief description of the shell model following Thewalt [82T] is

appropriate here. The lowest hole shell, labelled by Γ_8, has the four-fold degeneracy (including spin) of the Si valence band edge. The 1s electron shells are comprised of the valley-orbit states Γ_1 (doubly degenerate), Γ_3 (four-fold degenerate), and Γ_5 (six-fold degenerate). The ordering of the valley-orbit states for the BMECs was assumed to be the same as for the isolated donors, and the splittings were assumed to be negligible for acceptor complexes. The filling of electron or hole shells was expected to produce very stable complexes, and further, was used to explain patterns in the relative intensities of the BMEC lines observed in the PL series. Since a closed shell was assumed to have a small capture cross-section for an additional FE, the next, larger BMEC transition was expected to be much less intense. This type of pattern was observed for several BE-BMEC systems.

Until recently, only BMECs associated with substitutional donors and acceptors in Si were observed, although no theoretical argument precludes isoelectronic centers from binding more than one exciton. The very similar O and O′ centers [86T,87Sb] studied in Chapters 4 and 5 of this thesis are the first IBE-BMEC systems observed in Si. Since no model for these isoelectronic centers exists, however, it has not been possible to construct a shell-model description of the BMECs.

CHAPTER 2: PHOTOLUMINESCENCE EXPERIMENTAL METHODS

2.1: INTRODUCTION

The study of excitons in semiconductors using photoluminescence spectroscopy has become a useful materials characterization technique [87Ma] and is still of great importance in basic semiconductor research. [88D] Most of the experiments on Si reported in this thesis were carried out using standard PL methods which have been described in detail previously [83W, 86Sc, 86Wc, 88C] and are briefly summarized in this chapter for completeness. The polyexciton experiments, which were performed near twice the Si band gap using a data acquisition system featuring an imaging photomultiplier tube [88M], are described in the experimental section of Chapter 6.

2.2: Sample Preparation and Experimental Methods

Two different He cryostats were used in these experiments. A standard Janis immersion dewar with an approximate optical aperture of $\cong$ f/3 was used for the ordinary continuous-wave and time-resolved PL, for the PL excitation (PLE), and for the stress experiments on the O-center (Chapter 4). By pumping on the sample chamber with a large vacuum pump, the sample temperature could be lowered below the He lambda point to as low as 1.6 K, as determined by the vapor pressure above the liquid. For higher temperature measurements, an Andonian variable temperature dewar was employed, in which the sample chamber is cooled by a continuous flow of cold He gas from a liquid He reservoir. A resistive heater was used to stabilize the temperature, which was determined by a Si diode sensor (Lakeshore DT-500-CU-36) mounted in close proximity to the sample.

The samples used both in the thermal donors study and in the investigation of the O and O′ isoelectronic centers were prepared from oxygen-doped Si grown by either the Czochralski (Cz) or float zone (FZ) method. In the Cz material, oxygen from the SiO_2 crucible dissolves in the liquid Si, and the resulting single crystal boule is highly oxygen doped. This unintentional and unavoidable O-doping of Cz Si, which is used extensively in device production, accounts for the technological importance of obtaining a quantitative understanding of the TDs. Our starting Cz material had $[O_i] = 7.5 \times 10^{17}$ cm^{-3}, as determined from the 9 μm IR absorption band. [73G] Residual donor (phosphorus) and acceptor (boron) concentrations as determined from PL [87Ma] were $[P] = 1.2 \times 10^{13}$ cm^{-3} and

[B] = 2.7 × 10^{12} cm^{-3}, respectively. Two adjacent 2 mm-thick slices from the seed end of a 4" - diameter Cz boule pulled in the <001> direction were diced on a diamond saw into samples approximately 6 mm by 12 mm. Two complete sets, having 13 samples each, were annealed in air at both 450 °C and 500 °C, using a three stage furnace with regulated temperature control. A chromel-constantan thermocouple was used to verify independently the furnace temperature in the region containing the samples. Annealing times of 0.25, 0.5, 1, 2, 4, 8, 16, 32, 64, 128, 256, 512, and 1024 hours were chosen to facilitate PL intensity *versus* annealing time measurements, which were expected to exhibit the same power-law dependence observed for the IR absorption spectra.

In order to study these systems in oxygen-doped FZ Si, we obtained a 1" - diameter 4 kΩ-cm boule which had been given a single pass in an oxygen atmosphere. The resulting material had $[O_i]$ = 8.1 × 10^{17} cm^{-3} at the tang end. Because of this extremely high doping level, some parts near this end of the boule were observed to be polycrystaline. A limited number of smaller 1.5 mm by 2 mm by 10 mm samples was cut from the single crystalline portion of this highly doped region, and three annealed samples were made. Annealing in air was done at 480 °C as described above, for 24, 48, and 72 hours, respectively. A similar set of samples cut from the middle of the boule, which contained $[O_i]$ = 3.0 × 10^{17} cm^{-3} was also prepared, but it did not show PL from the TDs.

Because of the interplay of annealing temperature and initial $[O_i]$ in the formation rate of the various TD species, different temperatures were used in the sample preparation. At each stage of the evolution, the 500 °C samples gave cleaner PL than their 450 °C counterparts, which contained a

more noticeable broad background underlying the resolved structure. The 500 °C set of Cz samples evolved more quickly than the 450 °C set obtained from the same material, however, which reduced the duration of the important short-annealing-time differences in relative TD concentration. The choice of 480 °C for the FZ material was a way of compromising the quicker evolution and the smaller background effects.

After receiving the appropriate annealing, all of the samples were cleaned and heavily etched in 10% $HF:HNO_3$ (CP4). This chemical etch removed approximately 50 μm of material from the surface of the samples, eliminating the "denuded" zone, which contains almost no TDs due to segregation of the TDs away from the surface.

The samples were cleaned with acetone and ethanol to remove any grease, and were mounted in a strain free manner onto a sample holder by wrapping them with teflon tape. As many as twenty samples could be placed in the immersion dewar at one time, while the variable temperature dewar held a maximum of four samples. Care was taken to ensure that no excessive tension was applied to the teflon tape, since this produced broadened PL lines due to the effects of stress on the band edges.

Excitation was provided by a variety of laser sources, including the 514.5 nm line of an Ar^+ ion laser, and a 200 mW infrared diode laser which peaked near 800 nm. The thermal donor bound exciton luminescence was stronger when the longer wavelength diode was used as the excitation source, probably because of its greater absorption depth in Si. The strong signal from the O- and O'-centers was easily observed using the green line of the Ar^+ laser.

For the time resolved measurements, the output from a pulsed GaAs diode array, or a dye laser using Rhodamine 640 dye (operated at ≅ 625 nm) under Nd:YAG excitation, or an Ar^+-pumped mode-locked cavity-dumped dye-laser (also operated near 625 nm) was used. These sources allowed short and long lifetimes to be measured, since the pulse rates were different: typical repetition rates were 4 MHz or 800 kHz for the Ar^+ - pumped dye laser, and 1 kHz for the Nd:YAG - pumped dye laser or the pulsed diode array. The range of lifetimes in the study of the O-lines was the greatest, going from as long as 85 μs for the principal line at 1.6 K to as short as 8 ns for the O^4 transition.

The tunable near-infrared laser excitation used in the PLE experiments on the principal O and O′ lines described in Chapters 4 and 5 was provided by an optical parametric oscillator (OPO) which has been described in detail by Watkins.[86Wc] The non-linear crystal used in this OPO was $LiNbO_3$, which was pumped by a tunable dye laser. Typical dye laser powers of 400-450 mW at 625 nm and 2 kHz were used, resulting in an OPO power of approximately 30 to 70 mW. Using a single set of mirrors in the OPO cavity, a tuning range from 1.0 to 1.180 μm was achieved with excellent pulse-to-pulse stability. The PLE spectra were collected by monitoring the luminescence at a single wavelength and scanning the excitation to shorter wavelengths under computer control. In order to observe the ground state in PLE, a mechanical chopper synchronous with the OPO pulses was used to block the excitation but pass the long-lived luminescence.

The PL signal was collected from the sample and focused onto the entrance slit of a 0.75 m Spex double spectrometer equipped with 600 lines/mm gratings blazed for 1 μm. In order to calibrate the

spectrometer at the beginning of each day, the Hg line at 1.128740 μm from the fluorescent room lights was used. With a slit width of 100 μm, the spectral resolution of the spectrometer, as determined by the full width at half maximum of the Hg line, was typically 0.13 meV, and calibration accuracy was to within 0.01 meV. Some lower resolution spectra were collected with slit widths of 200 or 500 μm, resulting in spectral resolutions approximately 2 or 4 times lower than this. The spectrometer position was controlled by a customized computer program [86Sc], and was very reproducible: at the end of the day, very little (0.01 meV at the Hg reference wavelength) or no drift at all could be detected.

The luminescence was usually detected with a Varian VPM159A photomultiplier tube cooled to -100 °C, operated in photon counting mode. This detector is ideally suited for Si luminescence in the no phonon and phonon-assisted regions, and has a long wavelength cutoff near 1.2 μm. For longer wavelength spectroscopy, a North Coast intrinsic Ge detector, model E0817L, which is useful to 1.7 μm, was used. The analog signal from the Ge detector was processed using standard lock-in techniques. In the exciton region the signal-to-noise ratio of the photomultiplier tube was considerably better than that obtained under identical conditions using the Ge detector, and so the tube was used for most of this work.

Some spectra of the thermal donor bound exciton luminescence were collected using a Bruker IFS 113 Fourier transform interferometer. A fast Ge detector (North Coast E0817S) was used to detect the luminescence, which was collected at typically 1 cm^{-1} resolution using a Si-coated beamsplitter, efficient from 1000 to 10000 cm^{-1}. The application of Fourier transform spectrometry to photoluminescence was summarized recently

by McL Colley and Lightowlers. [87Ma]

Unfortunately, the Bruker interferometer is less than ideal near 10000 cm^{-1}, where the Si luminescence occurs, because of limitations on the mirror alignment, and so this parallel collection technique was not employed to full advantage: spectra of the relatively weak no phonon lines from the thermal donor bound excitons collected on the grating spectrometer system using the photomultiplier tube required a similar amount of averaging time to achieve the same signal-to-noise ratio.

CHAPTER 3: THERMAL DONOR BOUND EXCITONS

3.1: INTRODUCTION

The observation of shallow donor formation and subsequent annihilation in Czochralski (Cz)-grown Si subjected to thermal treatments near 450 °C is over 30 years old. [54F,57F] Because the solubility of oxygen in liquid Si is much higher than in solid Si, the boule pulled from a molten Si supply contained in an SiO_2 crucible is highly supersaturated with oxygen. Typical values for the interstitial oxygen concentration, $[O_i]$, in Cz Si are in the low- to mid-10^{17} cm^{-3} range. The requirement of a large initial concentration of interstitial oxygen in the Si for the donor formation was recognized from the start. [54F]

The first model for the thermal donors (TDs) due to Kaiser *et al.* (KFR) [58K] was constructed to explain the kinetics of donor formation and its dependence on the initial $[O_i]$. The formation rate of donors was found to be approximately proportional to the fourth power of $[O_i]$, [57K] and the maximum donor concentration observed in a plot *versus* annealing time was found to be proportional to the cube of $[O_i]$. [58K] These observations led KFR to propose that the so-called oxygen donor consisted of clusters containing four oxygen atoms.

Fuller and Logan [57F] also observed a reduction in donor concentration with increased annealing time, or with higher temperature anneals at > 800 °C. This phenomenon was explained in the KFR model by proposing that the addition of a fifth oxygen atom to the cluster

neutralized its electrical activity. Although successful in describing both the growth kinetics and disappearance of the oxygen donor, the KFR model predicts a much lower total donor concentration than is observed, unless an anomalously high oxygen diffusivity is invoked. [58K]

Infrared (IR) absorption measurements added detail to the experimental description of the formation of the TDs beyond that obtained by simple resistivity measurements. Wruck and Gaworzewski [79Wb] showed that the complicated absorption spectrum of annealed Si [72Ba, 58H, 75G, 77Ha] could be interpreted as a superposition of at least four separate double donor spectra, with absorption into both the neutral donors (TD_n^0) and singly ionized donors (TD_n^+) observed simultaneously. Further, they observed that new, successively shallower species of the double donors appeared in the material as the annealing time was increased. These shallower TDs increased in concentration at the expense of the species with higher ionization energies. Because the shallowest levels observed did not freeze out at very low temperature, they concluded that there were in fact four different TD species, and not just a single donor with a complex ground state manifold.

Grouping the neutral and ionized donors according to the observed ($2p_{\pm}$-$2p_0$) splittings, Wruck and Gaworzewski also showed that all of the TD species could be well described by effective mass theory [65K], and deduced ionization energies ranging from E_{TD}^0 = 69.5 to 62.55 meV and E_{TD}^+ = 154.9 to 136.7 meV, respectively.

More recently, Pajot *et al.* [83P] and Oeder and Wagner [83Oa] have extended this IR investigation and have shown independently that at least nine separate effective mass-like double donors appear sequentially in

thermally annealed oxygen-rich Cz Si as the annealing time increases. Table 3.1 gives the ionization energies for all species obtained by each of these three groups. The index n (n = 1 to 9) in the listing labels the different TD species, with a "ladder" of decreasing binding energies, which appear successively in the IR spectra as the annealing time is increased.

The clear and unambiguous identification of several TDs with different donor binding energies made the theory of KFR [58K] less compelling and gave rise to several new models regarding the chemical composition of the TDs. [830b, 840, 84C, 85N] In the main they propose that small aggregates of some atomic species, usually oxygen, increase in size with longer annealing time, and form the different TDs. The exact chemical nature of the TDs is still unknown, however, and none of these models will be discussed here.

By considering the effect of uniaxial stress upon the IR absorption spectrum of the TDs, Stavola *et al.* [85S] obtained important information about the site symmetry and ground state characteristics of the TDs. They showed that the donors have C_{2V} symmetry, and that the effective mass ground state wavefunction is constructed from only the two conduction band valleys along the C_2 axis of the defect. They also showed that the TDs contain some built-in stress, and are probably elongated structures aligned along the <110> crystal axis.

Several other experimental techniques have been used to study the TDs, including electron paramagnetic resonance (EPR) [78M, 87G], electron nuclear double resonance (ENDOR) [86M], deep level transient spectroscopy (DLTS) [81K, 83S, 86G] and Hall effect. [57F, 79G] The correlation in the behaviour of the observed signal with the resistivity or IR results *versus* annealing time was used to show that the centers under study are actually the TDs.

TD_n	E_{TD}^0 (meV)			E_{TD}^+ (meV)		
	Wruck	Pajot	Oeder	Wruck	Pajot	Oeder
1	69.5	69.1	69.3	154.9	156.3	156.3
2	67.0	66.7	66.9	149.1	150.0	149.7
3	64.7	64.4	64.7	143.6	144.2	143.8
4	62.55	62.1	62.3	137.6	138.5	138.2
5	-	60.1	60.2	-	133.1	132.5
6	-	58.0	58.1	-	128.5	127.9
7	-	56.2	56.5	-	124±1	-
8	-	54.3	54.1	-	121±2	-
9	-	52.9	53.0	-	118±3	-

Table 3.1: Summary of ionization energies of neutral and singly ionized thermal donor species, deduced from the effective mass approximation. All E_{TD}^0 obtained at 8 K. E_{TD}^+ obtained at 80 K (Wruck and Gaworzewski, [79Wb]) or 8 K (Pajot *et al.* [83P] and Oeder and Wagner [83Oa]).

The ENDOR and DLTS measurements also indicated centers with C_{2v} symmetry, in agreement with the IR-stress results of Stavola *et al.* [85S] The problem of correctly identifying the species using techniques other than IR absorption is not trivial, and is well illustrated by the EPR and ENDOR results: two separate spectra, the so-called NL-8 and NL-10 lines, have been interpreted as different stages of the TD sequence, and a variety of possibilities regarding the exact correlation with the TDs are still being considered. [86M, 87G, 88B]

All of the discussion thus far has been concerned with the experimental investigation of the double donors themselves. The ladder of TD ionization energies, their two charge states, the nature of the effective mass ground state manifold and the structural information on the defects have all been considered, and explored using various techniques, with good correlation between results obtained in different measurements. Using photoluminescence spectroscopy (PL) the bare donor cannot be studied directly, however, and the correlation with other experimental techniques, such as IR absorption, becomes more difficult. When excitons localized on the TDs recombine radiatively, transitions from the donor bound exciton system to the neutral donor may be observed, and photoluminescence (PL) may be used to investigate the excitonic system.

The first identification of a PL feature with the TDs was made by Tajima *et al.* [79Ta, 80Ta, 80Tb, 81T] who associated a broad featureless band in their "*B*-type" spectrum (from O-rich Si samples annealed for 64 h at 450 $^{\circ}$C) with the radiative decay of bound excitons (BE) localized on the TDs. We have obtained well-resolved PL results from the TD BE, and the results will be discussed in the following section.

3.2: Experimental Results and Discussion

The principal reasons for correlating the transitions seen in the excitonic region in PL with the TD absorption lines observed in IR spectroscopy [79Wb,83P,830a] are the identical dependence upon starting material and the behaviour with increasing annealing time: only in Si containing high initial concentrations of oxygen (and low concentrations of carbon) which have been annealed for several hours near 450 to 500 °C are the lines observed. Tajima *et al.* [80Ta] confirmed that the resistivity changed in their PL samples after annealing at 450 °C for 64 h, indicating donor concentrations approximately equal to 2×10^{16} cm^{-3}. In this sample they observed their *B*-type spectrum, which contained a band of luminescence in the no phonon (NP) region, and phonon replicas shifted to lower energy by both the TA and TO phonon energies. With a further 1 h anneal at 650 °C, the PL was completely quenched, in agreement with the destruction of the TDs at higher temperatures. From these results, Tajima *et al.* concluded that the PL components are associated with bound excitons (BE) localized on the TDs.

Figure 3.1 shows the 2 K PL spectra from two samples containing a well resolved series of lines in place of the PL band previously observed by Tajima *et al.* [80Ta]. The Cz sample was annealed for 32 h at 500 °C, at which time the PL from the TD BE was at its maximum. At the slightly lower temperature of 480 °C used for the FZ samples, which initially contained more O_i, the maximum TD PL intensity occurred after 72 h of annealing, and this sample spectrum is shown in the bottom of Figure 3.1. The PL spectrum

Figure 3.1

PL spectra from two annealed Si samples: Cz Si (top) and FZ Si (bottom). Both normalized to equal maximum peak height; the NP region has been enlarged by 10 x for clarity. Reproducible and well-resolved structure due to recombination of BE localized on the TDs is observed in each spectrum, with the large TO:NP intensity ratio indicative of binding to centers with extended potential wells rather than to simple point defects. The P and B BE transitions are observed clearly in the more strongly doped Cz material.

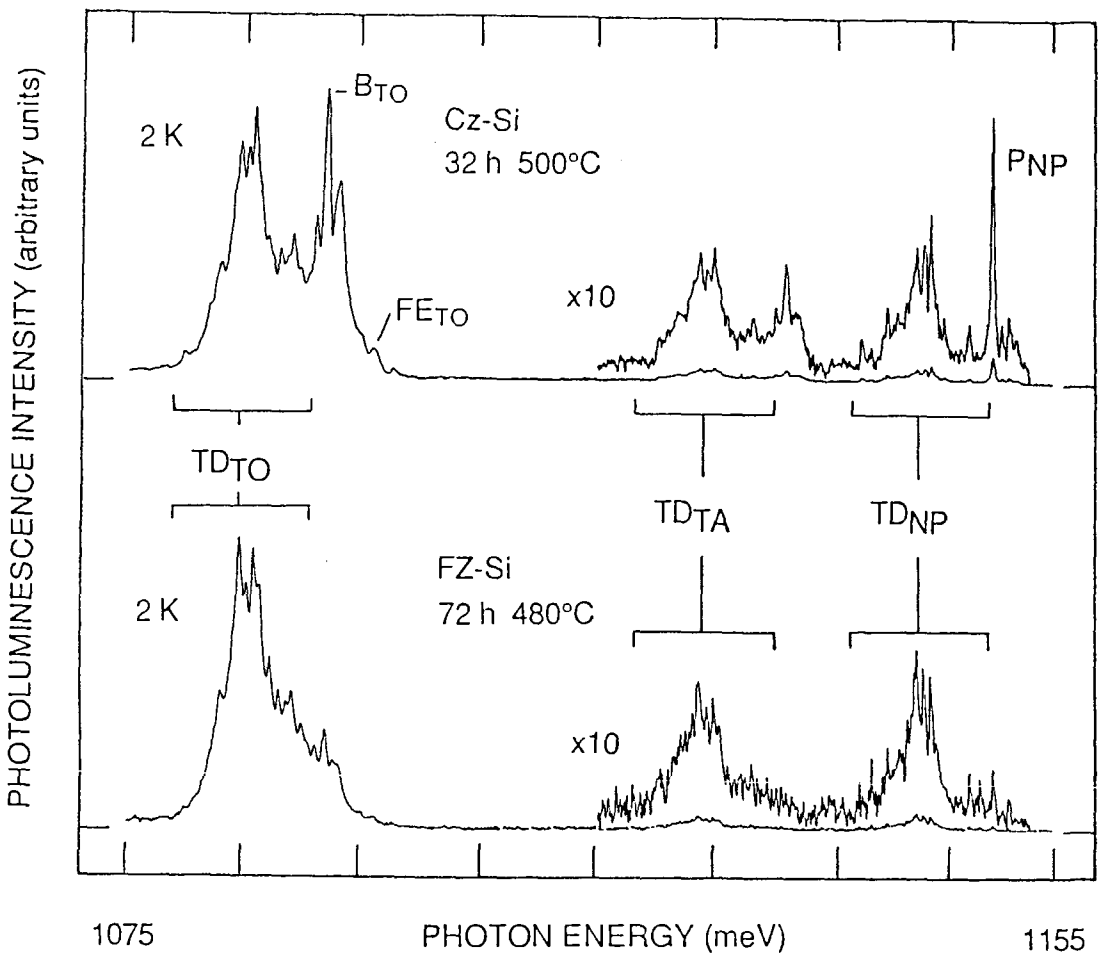
PHOTOLUMINESCENCE INTENSITY (arbitrary units)
2 K
B_{TO}
Cz-Si
32 h 500°C
P_{NP}
FE_{TO}
x10
TD_{TO}
TD_{TA}
TD_{NP}
FZ-Si
72 h 480°C
2 K
x10
1075
PHOTON ENERGY (meV)
1155

of TD BE is clearly reproduced in both types of starting material, with the very weak but well-resolved NP region being approximately 20 times less intense than the optical phonon assisted TO-replica. The very large TO:NP intensity ratio observed for these BE indicates binding to a center with an extended strain well potential, rather than to a point defect with a simple attractive short range central cell potential, since for other simple donor or acceptor BE with similar binding energies, the NP line is as strong or stronger than the phonon assisted recombination. This observation supports the association of these transitions with excitons localized on the TDs, which are known to have an anisotropic extended "central cell" potential [85S], and hence have reduced spatial localization and a corresponding reduction in zone-center *k*-component in the wavefunction.

The TO phonon replica of the free exciton (FE) recombination is indicated in Figure 3.1 by FE_{TO}, while the lines labelled P_{NP} and B_{TO} denote PL from the decay of excitons bound to these impurities. In spite of the lower signal levels, high resolution spectroscopy must be done in the NP region to avoid the phonon broadening and consequent loss of resolution inherent in examining the (more intense) TO replica. It is unfortunate that the TD PL is in the same spectral range as the luminescence from shallow BE associated with residual P and B, since this confuses an already complicated spectrum. Studies using ultrahigh purity FZ Si starting material doped with oxygen would help circumvent this difficulty. The spectra shown in Figure 3.1 contain at least 18 separate reproducible lines, and are consistent with the independent observations of Drakeford and Lightowlers [88D] in a PL study of heat treatments of Al-doped Cz Si.

Figure 3.2

High resolution NP spectrum of TD BE transitions with PL lifetimes for the principal transitions indicated. The long lifetimes for centers with these large exciton binding energies support the assignment of binding to the thermal donors, which are known to have extended potential wells. Two PL transitions are observed for each TD BE: the ground-state to ground-state transitions with exciton binding energies ranging from 3.8 to 11.5 meV, and ground-state to excited-state transitions shifted below these lines by the apparent valley orbit splitting.

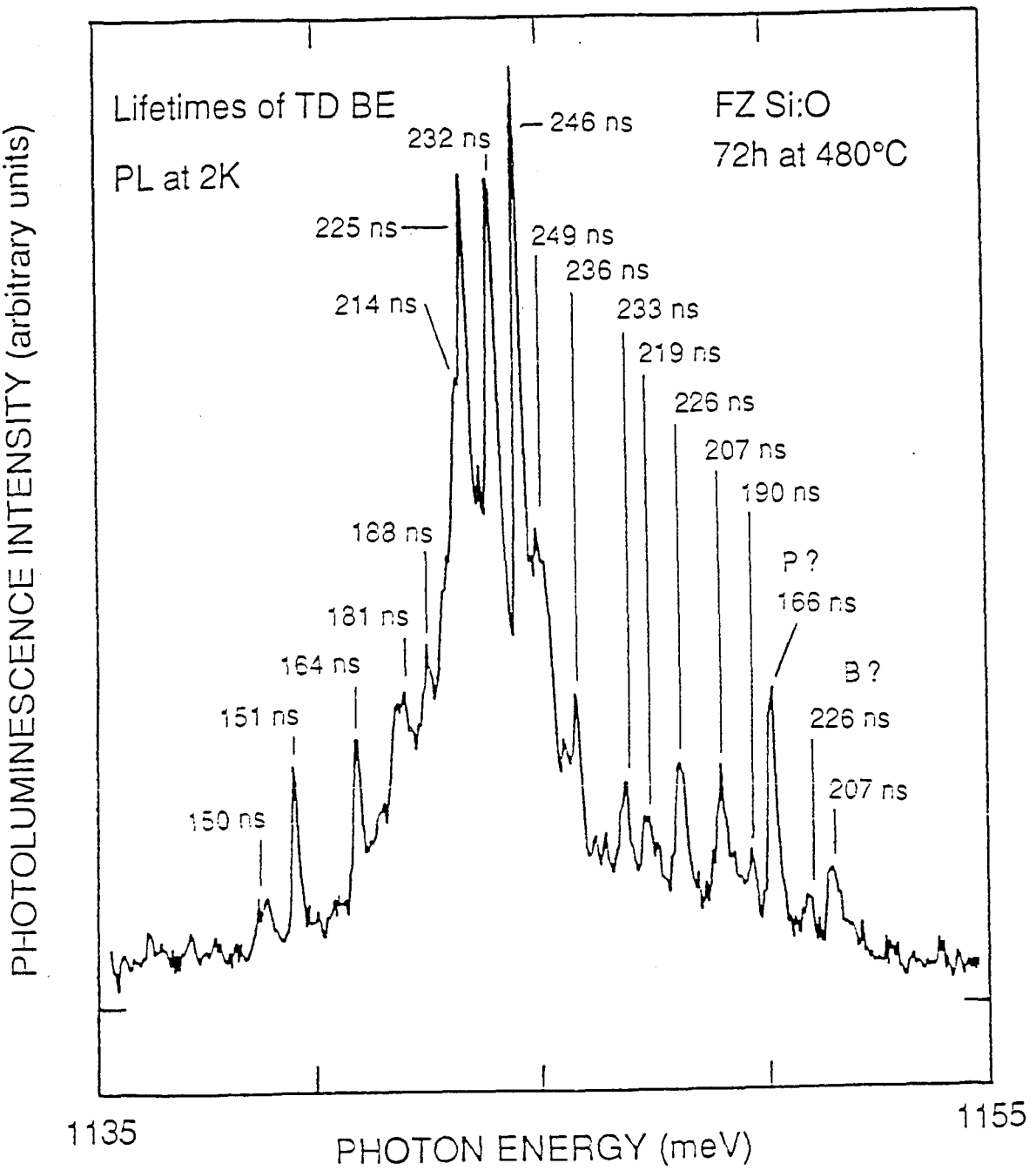
Lifetimes of TD BE
PL at 2K
FZ Si:O
72h at 480°C
246 ns
232 ns
225 ns
249 ns
236 ns
214 ns
233 ns
219 ns
226 ns
207 ns
190 ns
188 ns
P ?
166 ns
181 ns
164 ns
B ?
151 ns
226 ns
207 ns
150 ns
PHOTOLUMINESCENCE INTENSITY (arbitrary units)
1135
1155
PHOTON ENERGY (meV)

A high resolution NP spectrum showing greater detail is presented in Figure 3.2, with the BE PL lifetimes indicated for several readily identifiable transitions. The lifetimes were measured by collecting a histogram of PL intensity as a function of delay time after the exciting laser pulse and fitting an exponential to the decay. The hundreds of nanoseconds long lifetimes of the deeper lines are much longer than other BE in Si with similar binding energy: the deepest simple donor, Bi with exciton binding energy equal to 8.9 meV, has a PL lifetime of only 8.6 ns. [84S] The relatively long lifetimes observed for all transitions are consistent with localization by an extended potential well rather than by a short range central cell potential: the short lifetimes of deeper ordinary BE are due to the high Auger recombination rate, which depends strongly on central cell scattering. In addition, the trend in lifetime *versus* binding energy is not what one expects for BE localized on similar impurity centers. The luminescence lifetimes observed for excitons bound to neutral donors and acceptors are determined not by the radiative lifetime, but by the very fast, non-radiative Auger processes, which become more dominant with both increasing donor or acceptor binding energy and increasing exciton localization energy. Thus, the PL lifetimes are expected to become shorter as the luminescence energy decreases. Schmid has found that the Auger lifetimes of shallow BE in Si do in fact exhibit a power law dependence on the impurity ionization energy, and has concluded that for donor BE the relationship is $\tau_D \propto E_D^{-3.9}$ while for the acceptor BE it is $\tau_A \propto E_A^{-4.6}$. [77S] For the bound exciton PL transitions under discussion here, however, the lifetimes are seen to *increase* with decreasing PL energy from the highest transitions until the strong lines in the middle, and only

then do they begin to decrease with decreasing energy from there until the end of the series.

Further, there are at least 18 separate and reproducible transitions in the PL spectrum, while there are only nine identified species of TD. [83P] The explanation for both the number of lines observed in PL and their lifetime behaviour can be found by considering the effect of adding an *e-h* pair to a neutral TD. Since the effective mass wavefunctions for the TD electrons are composed from a *single pair* of conduction band minima, [85S] there are two doubly-degenerate electron states separated by the valley-orbit splitting in the ground state manifold of these double donors. When an exciton becomes localized on the neutral TD, there are a total of three electrons in the ground state, necessitating the occupation of both valley orbit states. An electron in either state can recombine with a hole and emit a photon, resulting in the possibility of *two* PL lines for a single TD BE species: the TD BE ground-state to TD ground-state transition separated from the FE edge by the exciton binding energy, and a TD BE ground-state to TD excited-state transition shifted below this line by the energy of the valley-orbit splitting. The latter transition leaves the TD in a final state with one electron in each of the two valley-orbit states.

These two transitions from the same initial state would have the same radiative lifetime as detected using PL. This trend is certainly evident in our spectrum of Figure 3.2. The pairing is not exact, however, and no firm identification of paired PL transitions can be made. The reason for this may involve the presence of some B and P in the FZ sample material. The lines labelled P? and B? in Figure 3.2 are located at the same energies as the BE transitions associated with these impurities, but the lifetimes

of 166 ns and 226 ns do not correspond to the known values of 245 ns and 1.0 μs, respectively, possibly indicating an accidental degeneracy with some TD BE transitions. It should also be noted that the two lines associated with a given TD BE will have the same PL dependence on sample temperature, and so should maintain a constant intensity ratio over some temperature range. Transitions involving different TDs will thermalize according to the binding energy of the weakly bound particle localized on the specific impurity center. Because of these facts, following the PL intensity *versus* temperature should enable the identification of PL pairs. Once again, however, the presence of B and P in our material made this identification inconclusive. From the figure and discussion, however, it is possible to tentatively assign all transitions to TD BE recombination, with exciton binding energies ranging from 3.8 to 11.5 meV.

Any discussion of the TDs would be incomplete without considering the annealing-time dependence of the series of donors. Models for TD production must account for the sequential introduction of successively shallower species with first ionization energies ranging from 69.3 to 53 meV. [83P] The implications for PL studies are quite clear, however, regardless of the chemical nature of the changing species. Since the PL intensity reflects the concentration of a given impurity species [87Ma], one expects the relative luminescence intensities from excitons bound to different TDs to change as the relative concentrations change with increased annealing time. This effect is demonstrated in Figure 3.3, where the seven NP spectra from the set of samples cut from the same Cz wafer and annealed at 500 °C for the times indicated are shown. All have been normalized to equal P intensity, and this feature has been scaled down by a

Figure 3.3

Annealing time dependence of the PL from TD BE for a set of identical Cz Si samples, normalized to equal P height. This strong feature has been scaled down by 1/2 for clarity. The P BE and BMEC lines are evident in the as grown material. The features due to recombination of excitons localized on the different TD species evolve at different rates, reaching an overall maximum in intensity near 32 h and then decreasing as other PL features appear. The behaviour is consistent with the known evolution and disappearance of the TD as observed in infrared absorption.

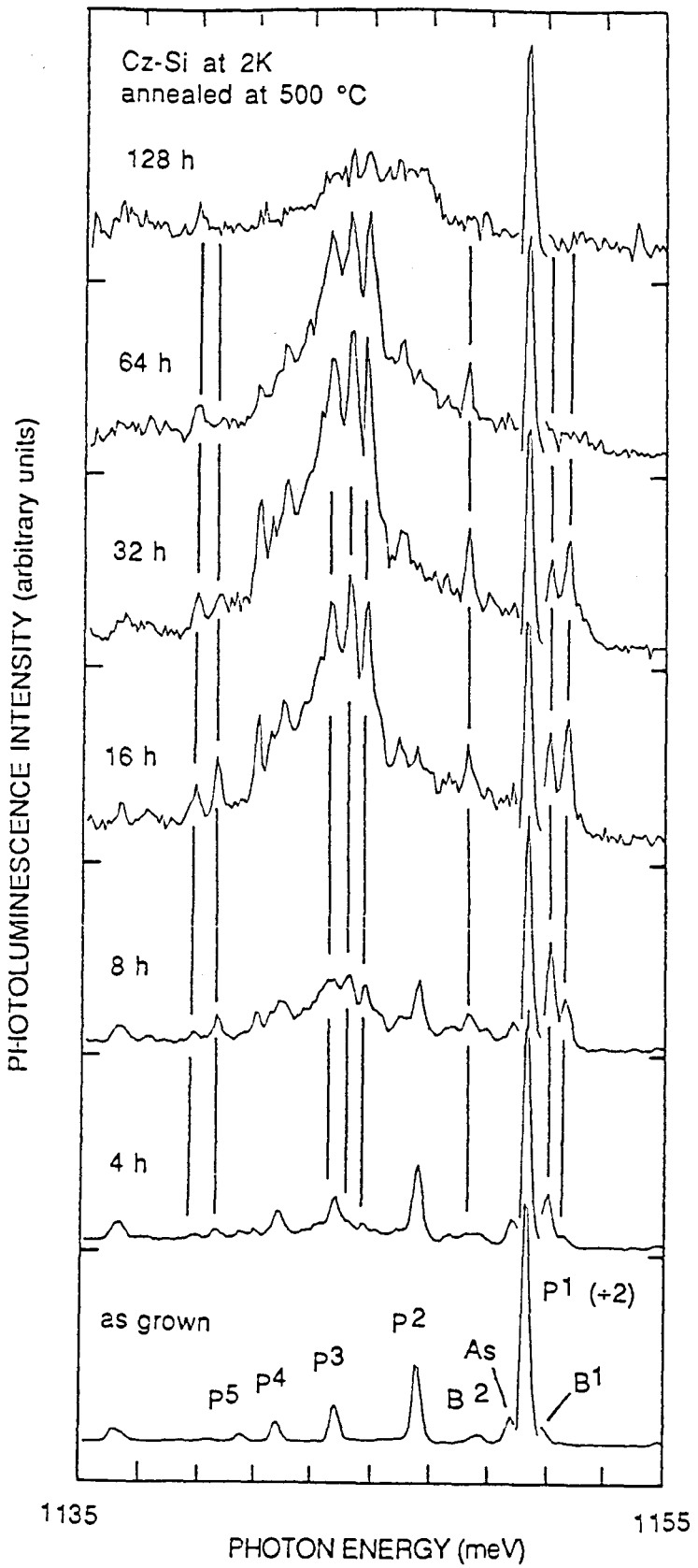
Cz-Si at 2K
annealed at 500 °C
128 h
64 h
32 h
16 h
8 h
4 h
as grown
P1 (÷2)
P2
P3
P4
P5
As
B 2
B1
PHOTOLUMINESCENCE INTENSITY (arbitrary units)
1135
1155
PHOTON ENERGY (meV)

36 b

factor of two for clarity. The lines labelled P^2 through P^5 in the as grown material are due to P bound multiexcitonic complexes (BMECs), with the superscript indicating the number of *e-h* pairs in the complex. [82T] The vertical lines show the evolution of some of the clearly resolved TD BE transitions as a function of annealing time, and it is clear that the relative intensities change for several of these BE species. The effects of thermal annealing are already apparent as early as in the 4 h spectrum, but the strongest features here are still due to P BMECs. Since it is at the earliest times in the annealing that the relative concentrations of the different TD species are changing most rapidly, PL experiments on UHP FZ Si doped with oxygen would be of critical importance in associating the transitions observed with specific TDs.

Also of interest in Figure 3.3 is the overall PL intensity from TD BE as a function of annealing time. For this material and annealing temperature, the spectrum increases in intensity until it reaches a maximum between 32 and 64 h, and then becomes less intense as other, deeper luminescence features appear and dominate the spectrum. The disappearance of the exciton luminescence correlates well with the known decrease and eventual disappearance of TD at long annealing times.

In order to investigate the behaviour of the TD BE excited state structure, PL excitation spectroscopy (PLE) was attempted. A tunable IR source was used to excite the 72 h 480 °C FZ Si sample at energies above the TD ground state transitions. Given strong absorption into the BE excited states and fast relaxation into the ground state, PL from the BE transition should increase in intensity as the laser is tuned to resonance with each successive excited state of the TD BE. The PLE spectrum obtained

in this manner is analogous to IR absorption, but subject to different selection rules. Unfortunately, due to the very small absorption coefficient for indirect BE, coupled with very low PL quantum efficiency due to Auger processes, this experiment did not work as planned, and no information on the exciton excited state series was obtained. The only observed signal for even the strongest BE line contained no structure, and was reproduced using excitation at *lower* energy than the ground state energy, indicating that some non-resonant or two-photon absorption process was the source of the PL. The relatively high peak power of typically 700 W from the pulsed excitation source makes it quite likely that the two-step two-photon processes dominate this experiment. A lower power continuous-wave excitation source would be required before the experiment could be usefully repeated, and even then the outcome is not certain due to the apparently weak absorption.

One other technique for confirming the donor nature of the binding centers in this study would be to look for the two-electron transitions, in which some of the energy from the recombining *e-h* pair is transferred in a partial Auger process to one of the remaining electrons, leaving the donor in an excited final state. The observed set of such two-electron transitions would then be shifted down in energy from the main PL transition by the excited state energies of the donor involved. This series could be used to deduce the donor binding energy in exactly the same manner as is used for IR absorption, and would in principle provide the correlation between the TD binding centers and the BE PL transitions. Once again, however, the PL signal was too weak to observe the two-electron

transitions in our samples, and no such correlation is possible on the basis of our results.

3.3: Conclusions

Clearly resolved PL transitions from BE localized on the different TD species have been observed and investigated using time resolved PL spectroscopy. Using the fact that the known effective mass ground-state for the electrons on the double donors is constructed from only two of the conduction band minima, the observation of at least 18 PL transitions with what at first appears to be unusual lifetime ordering has been explained. Support for the extended "central cell" potential is found in the large TO:NP intensity ratio seen in all PL spectra, further enhancing the identification of these BE with the TDs.

CHAPTER 4: THE O ISOELECTRONIC CENTER

4.1: INTRODUCTION

As discussed in the previous chapter, the evolution of the photoluminescence (PL) spectrum of oxygen-rich Si with increasing annealing time follows the observed behaviour of the thermal donors (TDs) observed in infrared (IR) absorption [83P] and resistivity experiments. [58K] The decrease in intensity of both the IR signal and the PL in the excitonic region after typically 64 h at 500 °C correlates with the resistivity behaviour at long annealing times, which indicates a decrease in the total TD concentration. In PL, however, two new luminescence features are observed to appear sequentially and increase in intensity at these long annealing times, and these will be discussed in this chapter and the next.

The results of PL and photoluminescence-excitation (PLE) spectroscopy on the first set of lines produced in high-O_i, low-C Si after extended heat treatments at 450°C-500°C are reported here. Our results cannot be reconciled with either of two proposed models explaining these lines in terms of the recombination of free holes with several neutral TD [86Wa], or in terms of donor-acceptor-pair luminescence involving the TDs and residual boron. [86D] Instead, we find that the main line is an inhomogeneously broadened isoelectronic-bound-exciton (IBE) transition. This binding center, and the very similar O′ center discussed in Chapter 5 are unique in that they can bind up to four electron-hole (*e-h*) pairs, thus explaining the multiplicity of lines. [86T] The only other isoelectronic center

capable of binding more than one *e-h* pair is nitrogen substituting for phosphorous in GaP, labelled by N_p, which binds at most two. [69M] Our model predicts a long lifetime for the IBE line, but very short lifetimes for the bound-multiexciton-complex (BMEC) [82T] lines, due to Auger processes. We have verified that these otherwise very similar lines do have vastly different lifetimes, ranging from 85 μs for the IBE to 8 ns for the four-exciton BMEC. We have also resolved a ground-state splitting of the IBE line which leads to a strong dependence of IBE lifetime on temperature, an effect already well known for other IBE systems. [67C]

4.2: Experimental Results and Discussion

Weber and Queisser (WQ) [86Wa] reported the first detailed results of PL experiments on the O-lines observed near 1.1175 eV. They observed four transitions and interpreted them as being due to free-to-bound transitions involving some of the neutral TDs (TD^0) and free holes (h), on the basis of the asymmetric line shape and the transition energies, which agreed with the known ionization energies of several neutral TDs. The tail to high energy observed in PL is explained in this model by the kinetic energy distribution of the free holes which can recombine with either donor bound electron. The low energy edge of each line was used to determine the ionization energy of the donor involved, and they obtained good agreement with the values of Pajot *et al.* [83P] In a subsequent paper by Weber et al., [86Wb] the main transition (their O_0) was reinterpreted as recombination between charged oxygen precipitates and spatially separated holes, while the other lines were still ascribed to free-to-bound (h, TD^0) recombination.

Dörnen and Hangleiter (DH) [86D] also studied the O-system, and on the basis of time-resolved and excitation-density-dependent measurements, concluded that the lines were due to donor-acceptor-pair recombination involving some of the neutral TDs and residual B which was clustered near the TDs. This model attempted to account for the wide range of lifetimes in the series, but lost the ability to predict the transition energies, which related the model of WQ [86Wa] with the TDs. The PL energy for

donor-acceptor pair recombination is given by:

$$E_{PL} = E_g - E_D - E_A + \frac{e^2}{\varepsilon r^2} \qquad .....(4.1)$$

where E_g is the band-gap energy, E_D and E_A are the donor and acceptor binding energies, respectively, e is the electron charge, ε is the static dielectric constant, and r is the pair separation. Since the pair separation is not fixed, a suitable combination of r and E_D can describe the observed luminescence, with an arbitrary choice of donor species. In this way, the donor-acceptor-pair model of DH loses its ability to predict the TD ionization energies from the PL spectrum.

In agreement with WQ [86Wa], we found that the maximum intensity of the lines corresponded only with high-O_i and low-C concentrations in the starting material, but not on the presence of group-III or -V dopants or with the initial conductivity type. Also in agreement with them, we found the new luminescence lines to have a long incubation period - in one set of samples the new lines could barely be observed after 48 h at 500°C, but reached a maximum and totally dominated the spectrum at 96 h, thereafter slowly decreasing in intensity as other luminescence systems appeared. This behaviour does *not* parallel the time-dependent TD concentration as measured by IR absorption, but instead correlates with the *decrease* of the TD concentrations after very long heat treatment.

The PL system under study here was observed previously by Minaev and Mudryi [81M] at rather low resolution (their lines 5 and 6), and also by Tajima *et al.* (Y_1 - Y_3 lines). [81T] Some representative PL spectra are shown in Figure 4.1. The O label used by WQ [86Wa] has been retained,

since the lines are clearly associated with O, but the details of the labels have been changed to correspond to our model. Their O_1, O_2, and O_3 lines become our O^1_B, O^3, and O^4 lines, where the superscript denotes the number of electron-hole (*e-h*) pairs in the initial state. WQ also refer to a fourth line, O_4, but it does not appear in their published spectra [86Wa] and we have never observed it. The energies of the peaks were found to be in excellent agreement with those given by WQ, and are summarized in Table 4.1, below.

The general shape of the O^1 line, with a tail towards higher energies is certainly reminiscent of what one expects for a free-hole to neutral-donor transition, as pointed out by WQ [86Wa]. There are, however, some problems with this interpretation of the line shape, such as the small but definite sample dependence of the half-width at fixed temperature, or the fact that the half-width is typically greater than 5 k_BT at 1.6 K. there is also the problem that such free-to-bound transitions are not observed for any other donors in moderately-doped Si at these low temperatures.

Line	Photon Energy (meV)
O^1_A	1117.05
O^1_B	1117.5
O^3	1115.8
O^4	1113.8

Table 4.1: Peak energies of the O-lines observed in PL.

Figure 4.1

(a)-(c) PL spectra at 4.2 K at three excitation levels; $I_0 \cong 12$ W/cm^2. (d), (e) PL spectra at a bath temperature of 1.8 K at two excitation levels. O^1_A is lower in (d) than in (e) as a result of sample heating. All spectra normalized to equal O^1_B height.

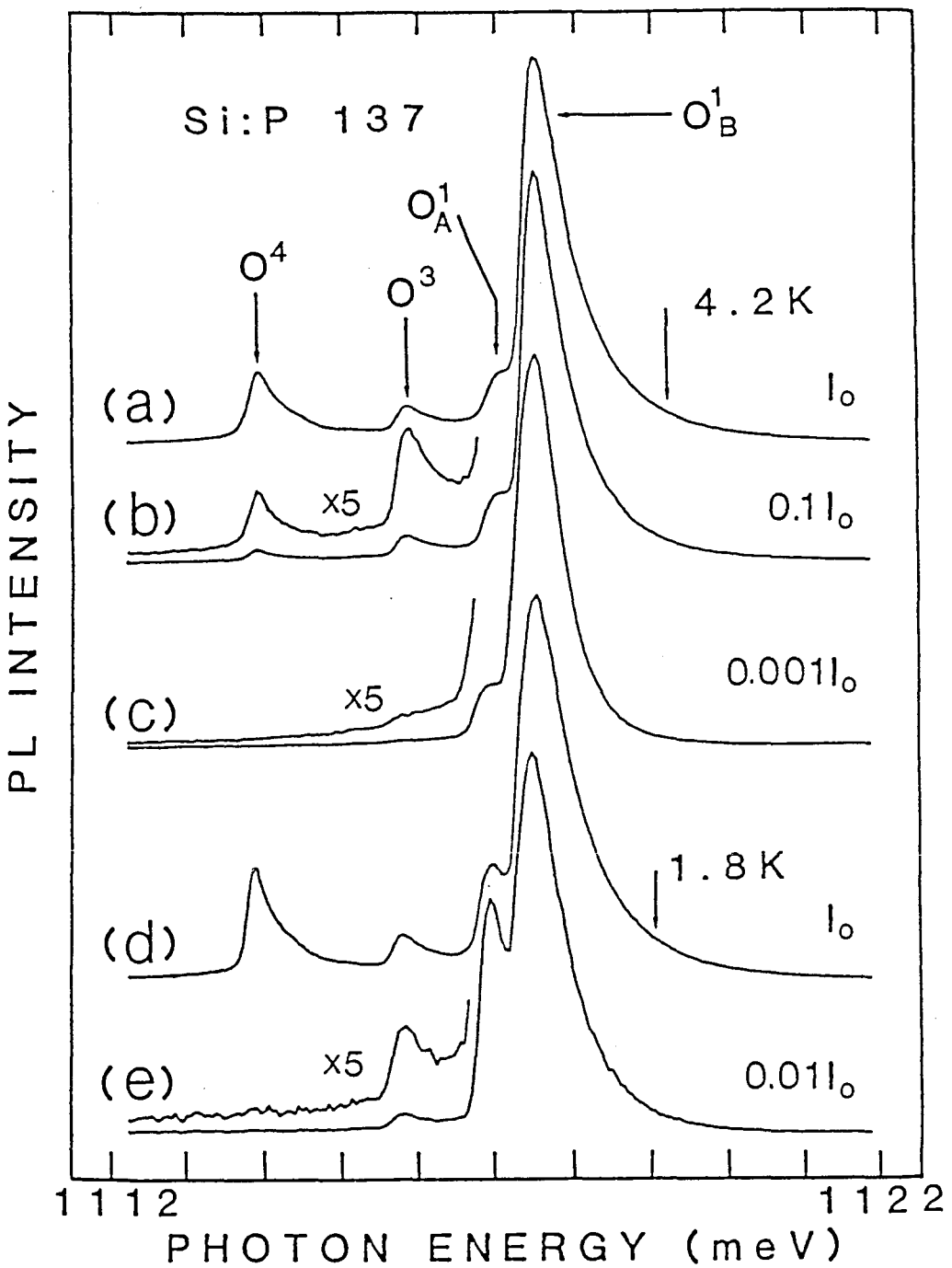
Si:P 137
O^1_B
O^1_A
O^4
O^3
4.2K
(a)
I_o
(b)
x5
$0.1I_o$
(c)
x5
$0.001I_o$
1.8K
(d)
I_o
(e)
x5
$0.01I_o$
PL INTENSITY
1112
1122
PHOTON ENERGY (meV)

We have observed a new, sample-independent splitting of the O^1 line into two components labeled O^1_A and O^1_B in Figure 4.1, and separated by ~ 0.45 meV. The two components are found to thermalize, indicating an initial-state splitting. The low oscillator strength of the O^1_A transition causes a strongly temperature-dependent lifetime for the O^1 line, as shown in Figure 4.2, since at low enough T most of the BE are "frozen" into the long-lived lowest lying O^1_A state. O^1_A and O^1_B have identical transient behaviour at all temperatures, indicating that the O^1_A - O^1_B system remains in thermal equilibrium. The lifetime of 85 μs at 1.6 K does not represent the low-temperature limit, since even at this temperature O^1_A and O^1_B are of roughly equal intensity. This splitting, and the resultant temperature dependence of the PL lifetime, are typical of IBE. [67C] They would be difficult to reconcile with the free-to-bound transitions proposed by WQ or the donor-acceptor pair transitions of DH.

The IBE interpretation is confirmed by our PLE results, some of which are shown in Figure 4.3. In Figure 4.3(a) the PLE spectrum is shown with the PL being detected over the entire, broadened O^1_B line. The PLE spectrum of O^1_B itself is seen to have the same shape as the O^1_B PL line, but to be considerably broader. O^1_A is not observed in PLE because of its low oscillator strength. A number of excited states are also observed, labeled O^1_C - O^1_F having the same asymmetric shape as O^1_B. This excited-state series is reminiscent of those previously observed for other IBE. [67C] Such an excitation spectrum is not predicted in either the free-to-bound model or the donor-acceptor-pair model. Instead, for free-to-bound transitions, one expects to observe not discrete excited states, but rather an absorption edge at the ground state energy of the donor and absorption into

Figure 4.2

PL transient decay curves for the O-system. Note that the time scale used for (a) and (b) is 10^3 times longer than that used for (c)-(e). The horizontal markers are decades. (a) and (b) have been arbitrarily shifted from (c)-(e). (a),(b) Decay of the O^1 IBE line at 1.6 and 4.2 K under low excitation conditions, with decay times of 85 and 17 μs, respectively. (c)-(e) Fast transient decays measured at the peak of O^1_B, O^3, and O^4 under higher excitation conditions. (e) has been shifted down one decade for clarity. Exponential fits to the initial decay transients of (c), (d), and (e) yield lifetimes of 45, 33, and 8 ns, respectively.

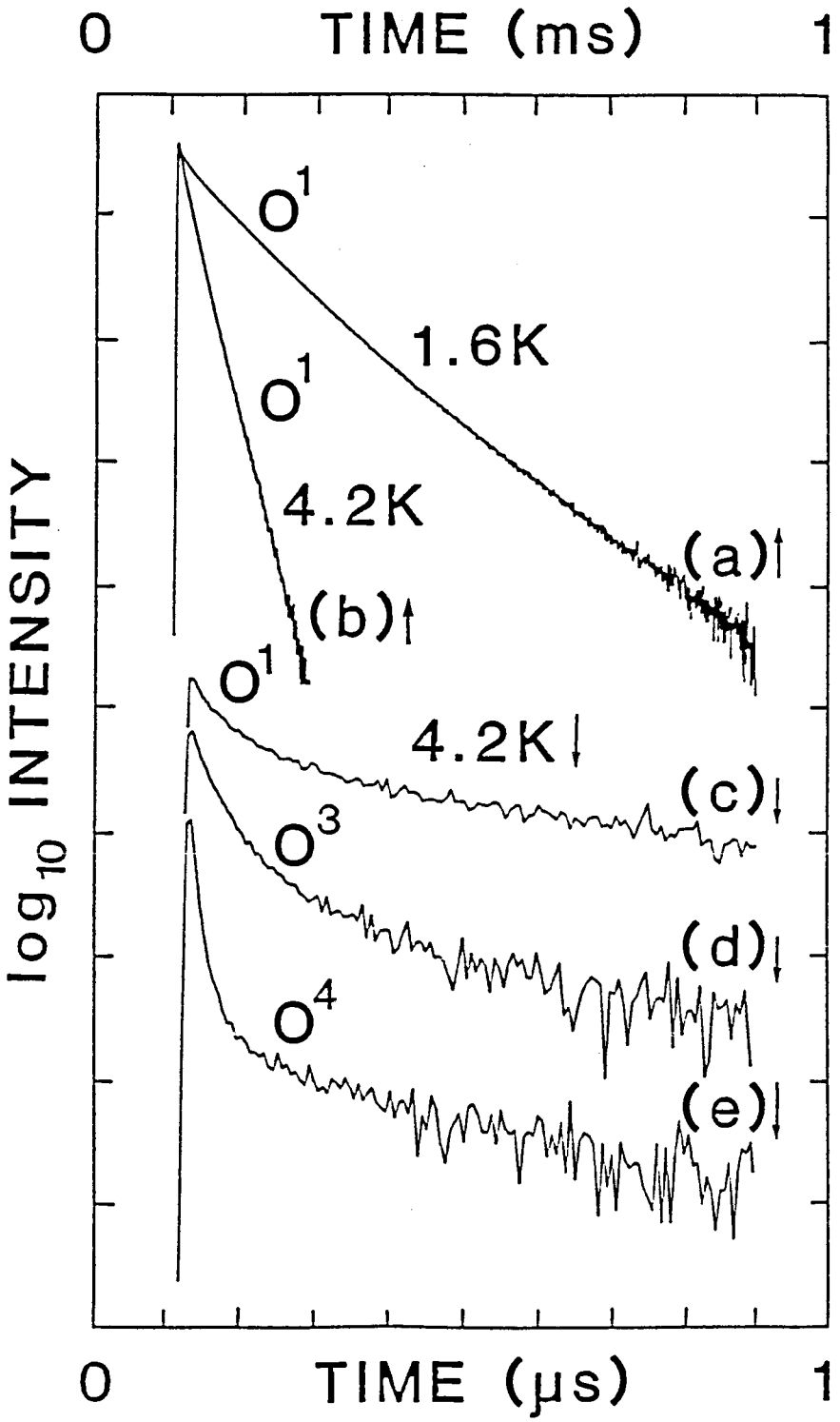
0
TIME (ms)
1
O^1
1.6K
O^1
4.2K
(a)
(b)
O^1
4.2K
(c)
O^3
(d)
O^4
(e)
$\log_{10}$ INTENSITY
0
TIME (μs)
1

Figure 4.3

(a) PLE spectrum of all O^1 states, including the O^1 ground state, with the PL signal detected over the entire, broadened O^1_B line. A mechanical chopper synchronized to the laser pulses prevented the direct detection of scattered excitation photons, but passed most of the long-lived luminescence signal. A number of excited states with the same asymmetric shape as the PL lines are observed. A signal is also observed due to excitation transfer from the P BE line in this sample, which contains 5 x 10^{15} cm^{-3} P. FE_{NP} marks the beginning of no-phonon free exciton absorption. The arrows labelled E_b indicate the range of thermally determined binding energies for O^1, which are in good agreement with the apparent ionization limit of the excited state spectrum. (c)-(e) Three PLE spectra taken with PL pickup in narrow bands, centered (c) at the peak of O^1_B, (d) 1.3 meV above the peak, and (e) 2.5 meV above the peak, as indicated on the PL spectrum (b). The PLE lines shift upwards in energy from (c) to (e), the signature of an inhomogeneously broadened distribution. The P_{NP} line is not observed in this undoped sample.

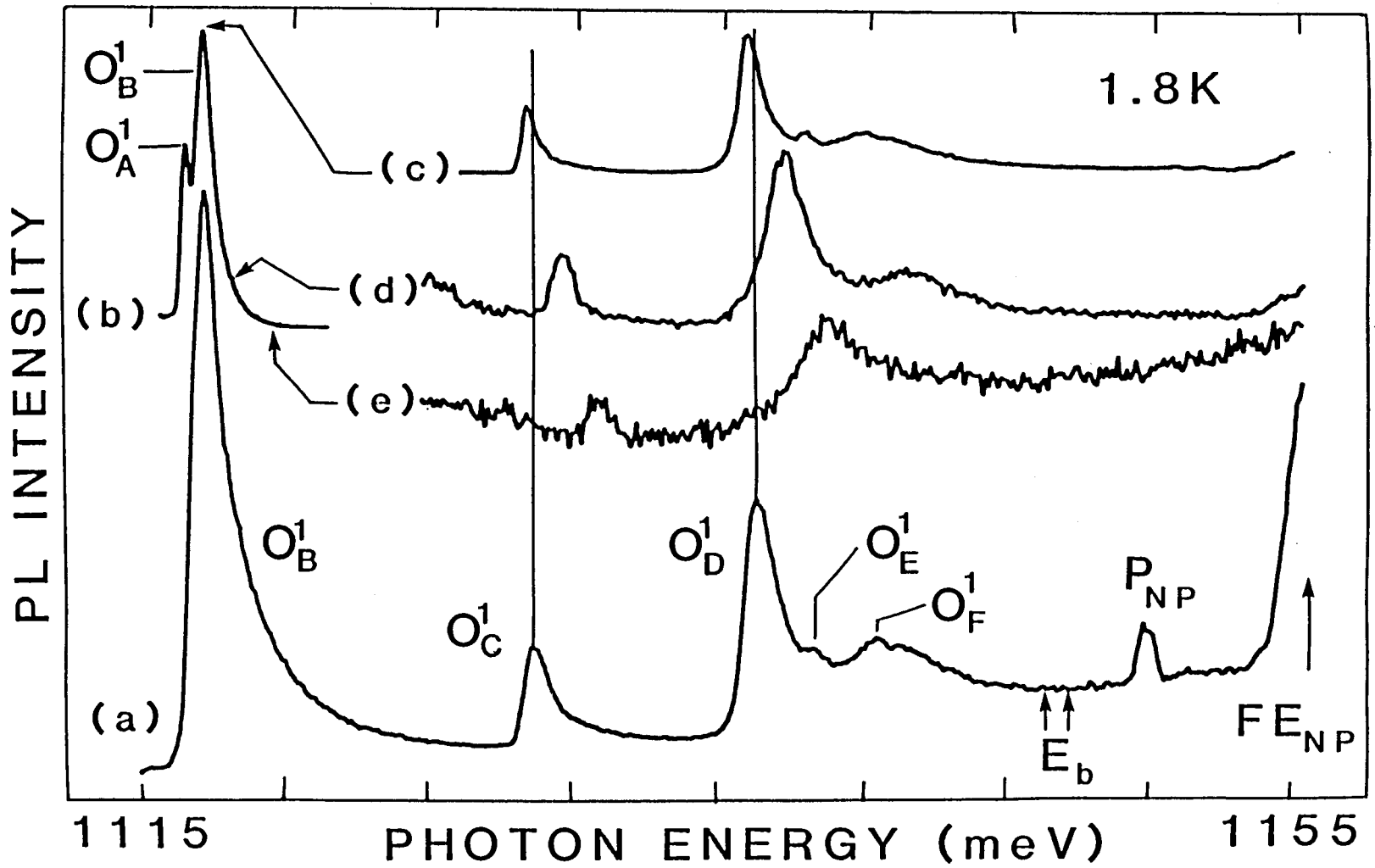
1.8K
O^1_B
O^1_A
(c)
(b)
(d)
(e)
(a)
O^1_B
O^1_C
O^1_D
O^1_E
O^1_F
P_{NP}
FE_{NP}
E_b
PL INTENSITY
1115
PHOTON ENERGY (meV)
1155

the continuum of free hole energies above it. While some structure may be expected in the excitation spectrum of donor-acceptor-pairs, it should be possible to assign all observed transitions to known excited states of the donor and acceptor. The ionization limit should reflect the shallower species in the pair. It should be pointed out, however, that while this approach is possible in theory, no such experiments have been successfully performed in Si. In any case, the observed O-related excited states do not match those of any known donors or acceptors in Si.

The excited state spectrum shown in Figure 4.3 appears to have an ionization limit at about 30 meV above O^1_A, which would thus be the predicted thermal quenching energy of the O^1 luminescence. This did not agree with the previously given value of 55 ± 3 meV, which supported the free-to-bound model.[86Wa] We have consequently remeasured the intensity of O^1 *versus* temperature for very low, moderate, and very high excitation levels. The plots of $\log[T^{3/2} \times (O^1 \text{ intensity})]$ *versus* 1/T, shown in Figure 4.4, yield straight lines of slope 30, 33, and 32 meV in the high-temperature limit. These values are in excellent agreement with the IBE thermal-dissociation energy predicted on the basis of the excited states detected in PLE spectra shown in Figure 4.3, but cannot be reconciled with the free-to-bound model.

The PLE spectra also reveal that the broadening mechanism which produces the unusual O^1 line shape has nothing to do with the kinetic energy of a free particle. As shown in Figures 4.3(c)-4.3(e), the PLE spectra change considerably when the PL signal is collected from different positions on the O^1 line. This is also true of PLE spectra taken of O^1 itself. The results show that the broadening results from an inhomogeneous

Figure 4.4

Arrhenius plots of PL from the O^1 transition in P-doped Cz Si annealed for 137 h at 500°C at three different excitation densities. The range of thermally determined binding energies from 30 - 33 meV obtained from the slopes of these plots is in good agreement with the apparent ionization limit of the excited state spectrum shown in Figure 9.

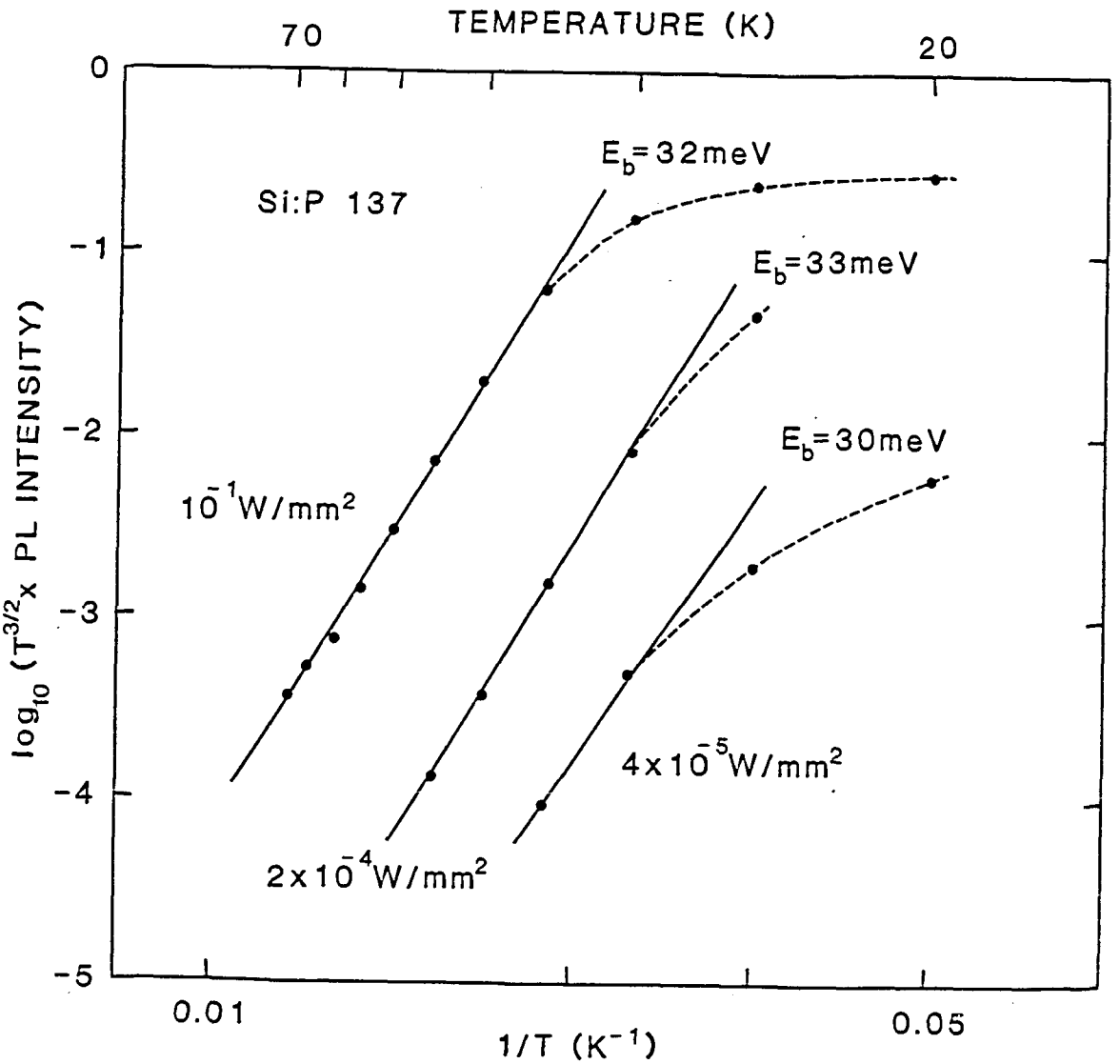
TEMPERATURE (K)
70
20
0
-1
-2
-3
-4
-5
Si:P 137
E_b=32meV
E_b=33meV
E_b=30meV
10^{-1}W/mm^2
2×10^{-4}W/mm^2
4×10^{-5}W/mm^2
$\log_{10}(T^{3/2}\times$ PL INTENSITY)
0.01
0.05
1/T (K^{-1})

distribution of binding centers having very similar shifts of ground-state and excited binding energies. It is also clear that the IBE created in the higher-energy tail of the distribution have a considerable probability of tunneling to lower energy before recombining. This explains the extra width of O_B^1 in PLE as compared to PL. As illustrated in Figure 4.5, the O_B^1 luminescence line shape changes with changing excitation energy. The narrowest line occurs for pumping directly into the <u>peak</u> of the O_D^1 excited state, while pumping with excitation tuned well out on the high energy tail of this excited state produces a much broader luminescence line shape, just as one expects for an inhomogeneously broadened distribution. The large probability of tunneling from IBE in the higher energy tail to lower energy is also verified by the observation that the measured O_B^1 lifetime decreases rapidly as one moves to higher energies along the PL tail. The inhomogeneous distribution could result either from random strains or from a distribution of very similar centers having slightly different total IBE binding energies. Since PL from other bound excitons (BE) in these samples, such as the P donor BE, is not broadened, the latter possibility seems most likely.

We will now consider the origin of the lines labeled O^4 and O^3 in Figure 4.1 (O_3 and O_2 of WQ). It was previously argued that since the relative intensities of O^1, O^3, and O^4 were somewhat sample dependent, they must originate from different centers. [86Wa] We instead find that the modest sample dependence of the relative intensities is exactly what one expects for a BE-BMEC system associated with a single center. [82T] In *all* samples one can observe $O^1 > O^4 > O^3$ at high excitation levels,

Figure 4.5

Excitation energy dependence of the O_B^1 luminescence line shape. (a) Non-resonant, above band-gap excitation. (b) Excitation resonant with the peak of the O_D^1 excited state. (c) Excitation 1.04 meV above the peak of the O_D^1 excited state. The narrowest O_B^1 luminescence line is observed in (b), with resonant excitation, indicative of an inhomogeneously broadened distribution.

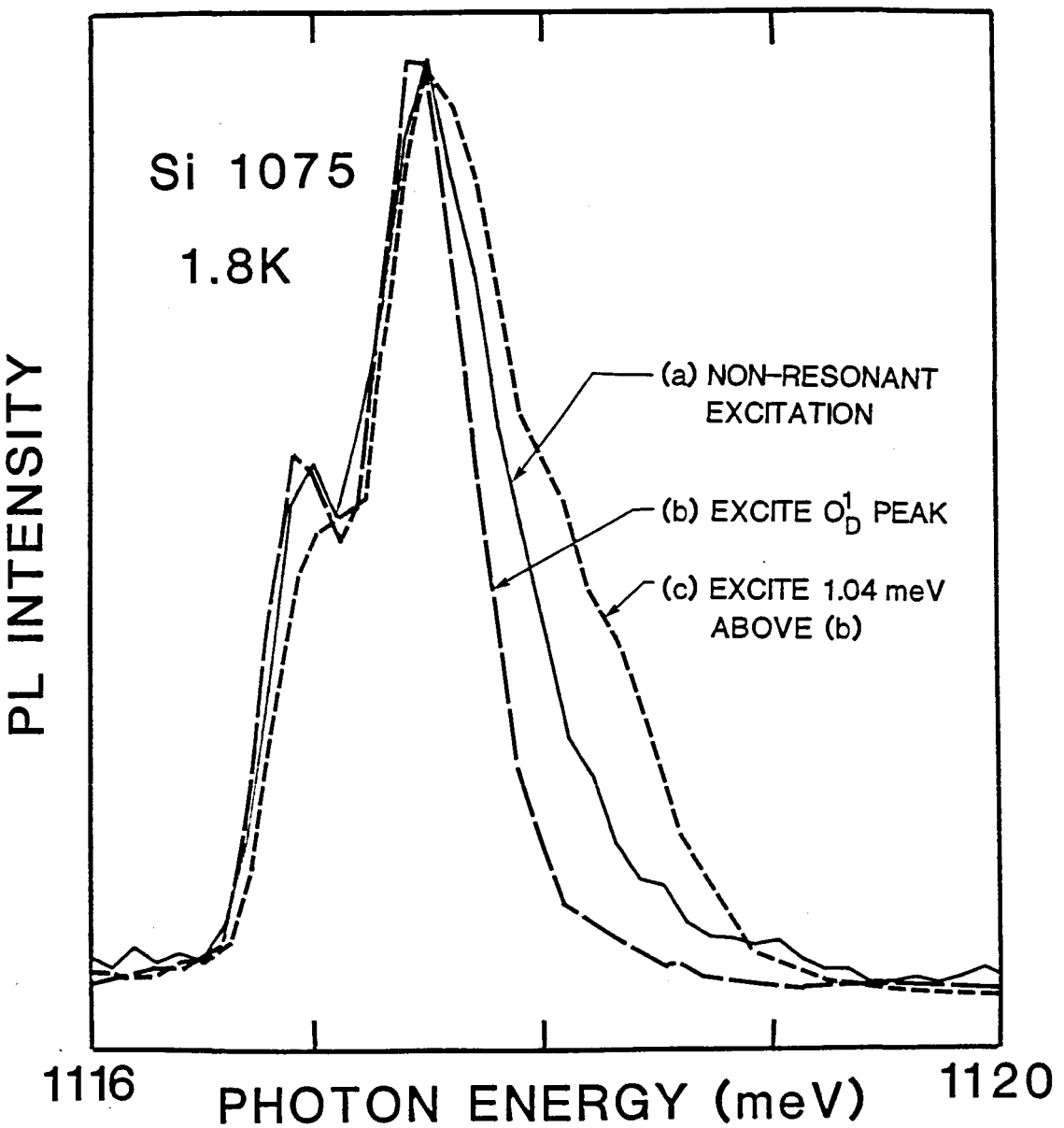
Si 1075
1.8K
(a) NON-RESONANT EXCITATION
(b) EXCITE O^1_D PEAK
(c) EXCITE 1.04 meV ABOVE (b)
PL INTENSITY
1116
PHOTON ENERGY (meV)
1120

$O^1 > O^3 > O^4$ at intermediate levels, followed by the disappearance of first O^4 and then O^3 at lower excitation.

The PL intensity dependence on excitation density of each of these lines, which is shown in Figure 4.6, is consistent with O^1 being a BE transition, while O^3 and O^4 are BMEC transitions, with O^4 having more bound *e-h* pairs than O^3. [82T] These more detailed measurements of line intensity *versus* excitation density show O^1 to vary as the 0.9 power of the excitation in the low-excitation limit, typical of a BE, while O^3 and O^4 vary as the 1.04 and 1.65 power of the excitation density respectively, typical of BMEC. The BMEC explanation of O^3 and O^4 is also supported by the fact that these lines, unlike O^1, cannot be created by resonant, subbandgap excitation.

Further support is provided by measurements of the PL lifetimes of O^3 and O^4. Typical decay curves are shown in Figures 4.2(d) and 4.2(e) - note that the time scale is 10^3 times shorter than that used to display the O^1 PL decay. These results were carefully checked for background effects by recording of complete spectra at various times after excitation. The O^3 and O^4 PL lifetimes, as determined by fitting of an exponential to the initial part of the decay curves, were 33 ns for O^3 and 8 ns for O^4. Longer decay times were observed at higher excitation levels. This and the slower, weaker tails on both the O^3 and O^4 decays are evidence for the saturation of free-exciton (FE) decay channels and the generation of new FE during the decay process itself, from the Auger dissociation of BMEC.

The surprising observation that O^3 and O^4 had lifetimes up to 10^4 times shorter than O^1, even though all the lines are clearly related, is readily explained in our BE-BMEC model. The BE (O^1) initial state contains

Figure 4.6

Excitation density dependence of the 4.2 K PL intensity of O^1, O^3, and O^4 lines. Fits to the low density limit show that the O^1 intensity varies as the 0.9 power of the excitation, typical of BE, while the O^3 and O^4 intensities vary as the 1.04 and 1.65 powers respectively, typical of BMEC.

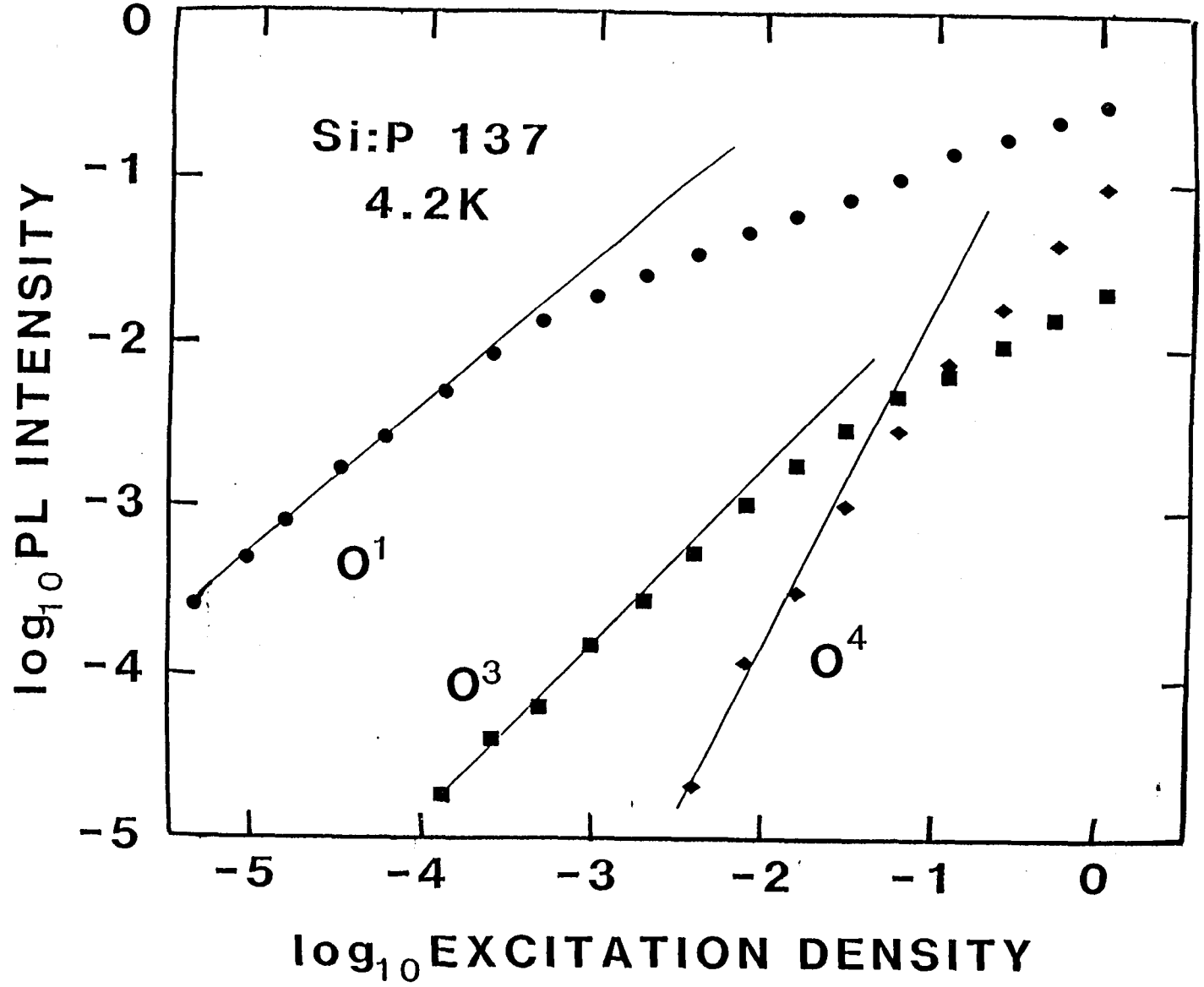
Si:P 137
4.2K
O1
O3
O4
log10PL INTENSITY
log10EXCITATION DENSITY
0
-1
-2
-3
-4
-5
-5
-4
-3
-2
-1
0

only one electron and one hole, and hence has the long lifetime typical of an IBE. The BMEC, on the other hand, have more than one bound *e-h* pair, and can decay by the non-radiative Auger process, which will be very rapid for these relatively tightly bound excitonic systems.

Although there is no direct evidence that O^3 and O^4 are transitions of BMEC's containing specifically three and four excitons, this seems the most likely scheme. Both the excitation intensity dependencies outlined in Figure 4.1, and the lifetimes shown in Figure 4.2, are consistent with O^4 having more bound *e-h* pairs in its initial state than O^3. The relative intensities of BMEC lines, and their binding energies, are very dependent on the filling of electron or hole shells, as described in Kirczenow's shell model. [77Ka,77Kb]

PL transient measurements provide an answer as to the location of the missing fourth line. At low excitation levels, or with resonant excitation, the O_B^1 line decays with its many-microseconds-long time constant right from t=0. However, at higher levels an initial rapid decay process, with a typical lifetime of ~ 45 ns, is observed to be superimposed over the much slower O^1 decay. It thus appears that a third BMEC line occurs at almost the same energy as O_B^1. Since the lifetime of this line is greater than that of O^3 and O^4, while its binding energy is less, it seems most probable that the hidden line is O^2, the two-exciton BMEC transition.

In order to confirm the BMEC interpretation, and to establish the location of the missing O^2 transition, PL experiments in the green near twice the Si band-gap energy were undertaken. The process giving rise to this luminescence signal involves the simultaneous recombination of two *e-h* pairs and the emission of only one photon. This approach has been used to

study the P BMEC series, [80S,85Tb] and it was hoped that the O-lines could be studied in this manner, since this type of transition cannot occur for donor-acceptor recombination, or for free-to-bound transitions. Unfortunately, however, this process is intrinsically very weak, and since the green photons are strongly reabsorbed by the Si, only a small sample volume very close to the crystal surface can be studied. No transitions corresponding to recombination associated with the O-center were observed in any of the samples we tried. In two UHP samples examined with this technique, however, resolved structure due to the recombination of free polyexcitons containing more than two *e-h* pairs was observed. [87Sa] These results are discussed in more detail in Chapter 6.

The last PL technique employed to study the system of O-lines was piezospectroscopy. The application of a uniaxial stress lowers the symmetry of the crystal, removing degeneracies and hence splitting observed transitions according to group-theoretical predictions. [65K] Any stress will split the fourfold degenerate valence band maximum into two doubly degenerate bands, while the six conduction band extrema behave differently under different applied stresses: <111> stress induces no splitting; <001> stress lowers the two minima along the stress axis and raises the four perpendicular to it; <011> raises the two minima perpendicular to the stress axis, and lowers the other four. These splittings are observed for FE recombination in Si, where the higher energy component corresponds to the recombination of an FE with its electron in one of the upper valleys (the "hot" FE), and the lower energy ("cold" FE) component is due to the electron being in one of the lower valleys. No additional components due to the valence band splitting are observed in PL since the holes can

thermalize without changing *k*-vector, and hence populate only the higher extremum when the splitting would be large enough to observe. When the applied stress is increased sufficiently, it becomes possible for intervalley electron scattering to occur via the emission of an acoustic phonon, and the hot component will be quenched. The conduction band minima are located along the six <100> directions 85.(3)% of the way to the Brillouin zone boundary, and the phonon with the appropriate wave vector for intervalley scattering has an energy of 18.5 meV.[72N] This would be the predicted maximum splitting of the FE components at which the hot FE could still be observed. Similar hot and cold luminescence components have been observed for acceptor BE [79Tb] where the intervalley mixing of the bound electron wavefunction due to the binding center is negligible. For this situation, the phonon-assisted intervalley scattering would still be expected to quench the hot PL and determine the maximum separation at which both components can be observed. In general, however, the piezospectroscopy of BE and BMECs is much more complicated, [79Tb] and will not be treated in detail here.

A sample from the same Cz Si boule used previously was cut into a parallelepiped with the long axis oriented along the <001> crystal axis. The orientation was accomplished using X-ray diffraction, and was to within 1°. The sample measured 1.850 by 3.405 by 16.0 mm, giving a surface area of 6.30 mm^2 for the application of the stress. After annealing for 72 h at 500 $^{\circ}C$, which produced enough of the O-centers for easy observation in PL, the sample was mounted into the jaws of a stress rig using double sided tape [86Wc] and inserted into the dewar tail for investigation at 4.2 K. The compressive stress was applied using a small-volume vacuum chamber and

a mechanical lever arrangement at the top of the rig, and a calibrated strain gauge provided a readout of the equivalent mass in kg. The stress on the sample was calculated from the sample surface area and the applied force.

Spectra of the O-center PL collected at several values of stress applied along the <001> crystal axis are shown in Figure 4.7. Two main components are observed to separate as the uniaxial stress is increased. The nature of the resolved structure in each component is not entirely clear. The lower energy component was broader at all values of the applied stress, possibly due to its greater sensitivity to stress inhomogeneities.

A fan diagram showing the peak luminescence energy of the O^1 transition as a function of stress along <001> is plotted in Figure 4.8, along with the FE data of Thewalt.[82T] Note that the energy scales have been shifted from one another: the O-line peaks are referenced to the lower scale, while the upper scale represents the energy at which the FE transitions would be observed in the no-phonon region, obtained by subtracting a single TO phonon energy from the observed PL.

The observed behavior of the O-line under <001> uniaxial stress is consistent with a model in which the bound electron wavefunction is composed only from a single pair of conduction band minima which has been shifted to lower energy than the two perpendicular pairs by some internal strain associated with the binding center. In this model, which is consistent with the known electronic structure of the TDs themselves [85S], the cold component of the luminescence corresponds to centers oriented such that the stress direction is parallel to the direction of the conduction band minima occupied by the electron, while the hot component corresponds

Figure 4.7

Spectra of the O-system at several values of externally applied uniaxial stress along the <001> crystal direction. Hot and cold luminescence components were observed even at the highest value of applied stress attainable in our experiment. The extra broadening of the cold (low energy) component may be due to its greater sensitivity to stress inhomogeneities.

O-system vs. <001> UNIAXIAL STRESS

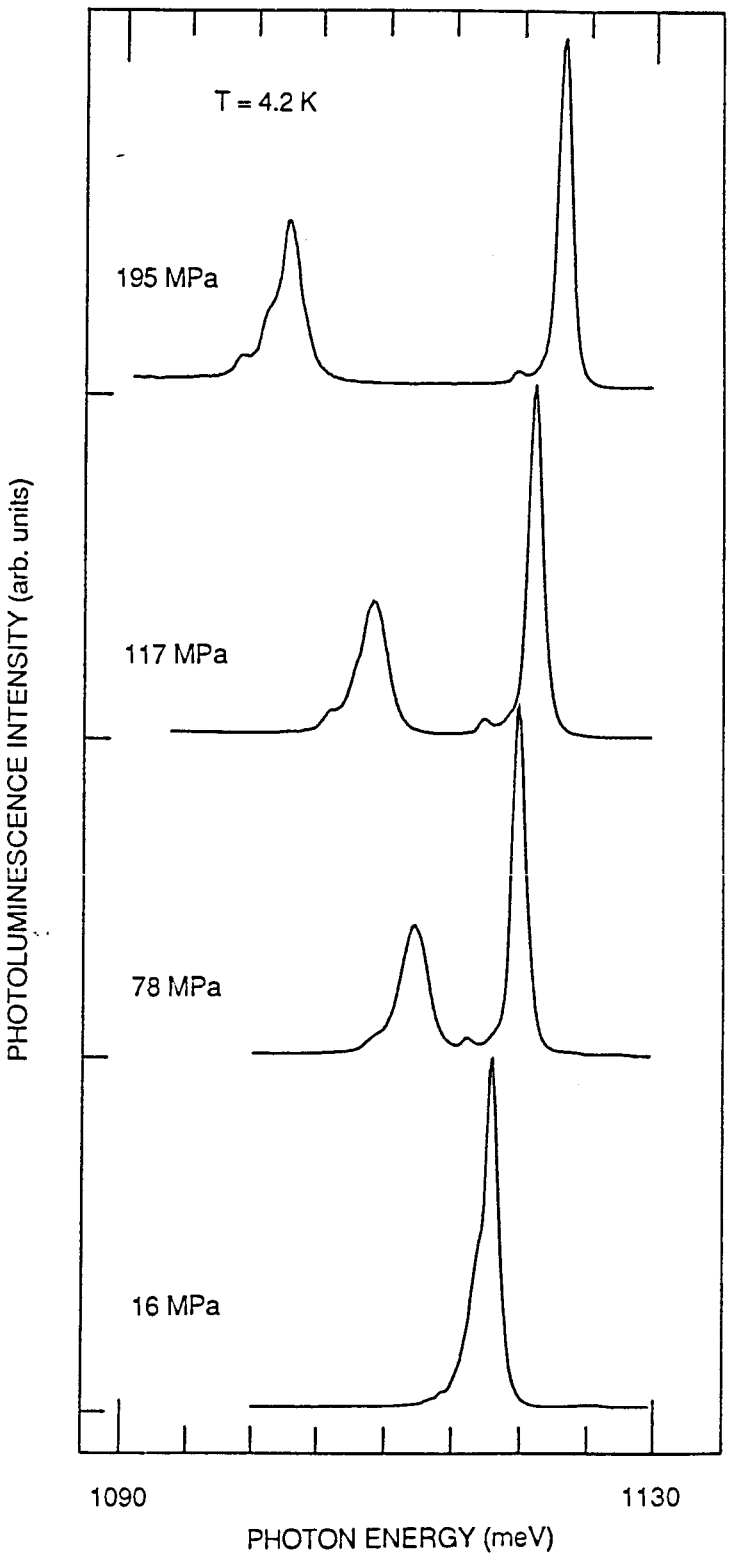

Figure 4.8

Fan diagram of the peak luminescence energy of the two components of the O^1 transition as a function of stress. The hot and cold free exciton components are also shown on the same scale. Note that the energy scales have been shifted for ease of presentation, and that the energy of the free exciton scale corresponds to the no-phonon region, obtained by subtracting one TO phonon energy from the observed FE transition. The persistence of the low energy O^1 component beyond the 18.5 meV threshold for intervalley scattering supports a model for the O^1 center in which the bound electron wavefunction is composed from only two conduction band minima.

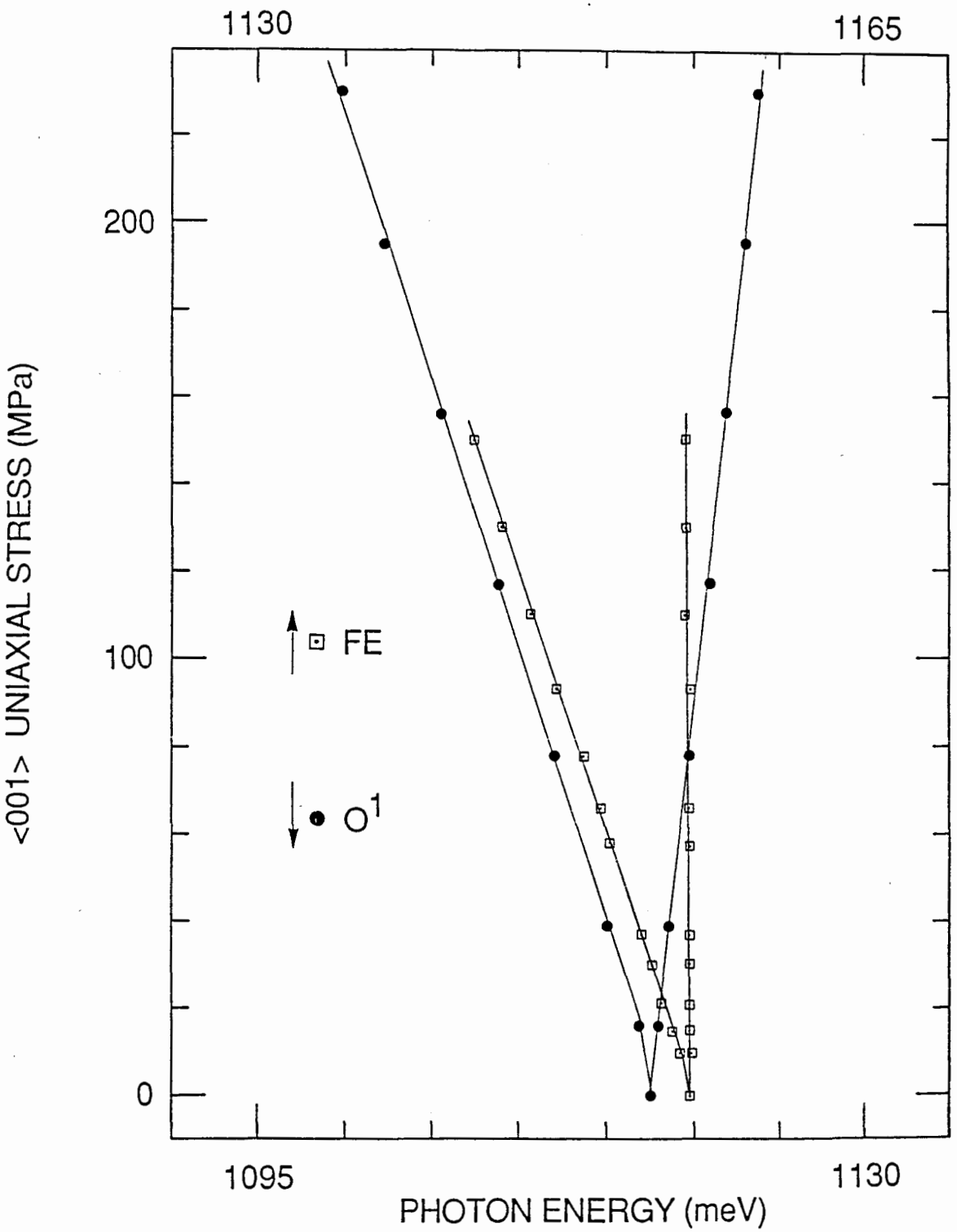
1130
1165
200
100
0
<001> UNIAXIAL STRESS (MPa)
FE
O1
1095
1130
PHOTON ENERGY (meV)

to centers oriented perpendicular to the applied stress. The principal experimental evidence for this model is the fact that the hot luminescence component is observed long after the stress-induced splitting exceeds the 18.5 meV threshold for intervalley scattering which applies in the case of initially equivalent conduction band extrema. In fact, we were unable to quench the hot component even with the application of 295 MPa of uniaxial stress along <001>, corresponding to a hot to cold separation of ≅ 32 meV, at which point the sample shattered and no further spectra could be collected.

The cold (parallel) component in the above model is expected to shift in the same manner as the cold FE, since the applied stress serves to lower the defect minima even further. This is indeed the case, as can be seen in Figure 4.8, where the O and FE cold components track quite closely.

On the other hand, the hot (perpendicular) component cannot be expected to follow the behaviour of the upper valleys in the FE case, since the applied stress acts in addition to the internal stress. In fact, the hot O component shifts to higher energy with increasing applied <001> stress more rapidly than the FE.

For the centers oriented perpendicular to the stress axis, the conduction band pair parallel to the stress axis must still shift to lower energy with increasing external stress, thus decreasing the splitting of the valleys associated with the internal stress. The quenching of the hot PL would then be expected at the point at which the minima parallel to the stress axis become degenerate with the minima along the defect axis, or at the point where intervalley mixing becomes important. This description is entirely qualitative, however, since no theory for the nature of the

exciton binding mechanism exists for the O-center.

4.3: CONCLUSIONS

We will now consider the possible origin of this unique isoelectronic binding center. The requirement of high O_i and low C concentrations in the starting material, along with heat treatment at 450 °C - 500 °C, are identical to those needed for TD generation. On the other hand, the long incubation period needed to produce this system shows that it does not grow in parallel with the TD population, but rather grows as the TD population *decreases* at long treatment times. We therefore propose that the new isoelectronic binding centers are the remnant cores of the TD after these lose their electrical activity through some reaction, the details of which are at present unknown. The inhomogeneous line width may result from the unresolved superposition of many similar centers having slightly different binding energies, similar to the TD themselves. [79Wb, 83P] The piezospectroscopic results indicate that the electronic wavefunctions are composed from a single pair of conduction band minima, in agreement with the known results for the TDs. [85S]

These results demonstrate conclusively that the new PL lines are associated with a BE-BMEC system localized on a broadened distribution of a single binding center. The agreement [86Wa] of the PL energies with those predicted for free-to-bound transitions involving three known TD species must be regarded as a coincidence. Stress- and Zeeman-splitting studies on the ground and excited states of the IBE would be most useful, with resonant excitation being used to eliminate the inhomogeneous broadening. The nature of the binding mechanism which produces this unique

isoelectronic BE-BMEC system also needs further study. Since the binding energies of all the species are almost identical, a rather extended "strain well" which, because of the stress results, may be considered to lower a single pair of conduction band minima seems a more likely possibility than the usual short-range central-cell binding mechanism.

CHAPTER 5: THE O' ISOELECTRONIC CENTER

5.1: INTRODUCTION

In Chapter 4 the spectroscopy of the O-lines seen near 1.175 eV in photoluminescence (PL) was considered in some detail, and a model was proposed which explained the main O^1 transition as the recombination of an exciton localized on an isoelectronic center, while the other two lines, O^3 and O^4, were ascribed to bound multiexcitonic complexes (BMECs) associated with the same center. A related group of lines, labelled by O' and observed near 1.052 eV, has also recently been observed in PL. [86D] The spectroscopy of this system, which parallels that of the O system already discussed, is reported in this chapter, and the same isoelectronic bound exciton (IBE) - BMEC interpretation is used to explain all of the observed luminescence.

The O'-lines were first observed by Weber and Queisser (WQ) [86Wa], who saw only the main transition and ascribed it to the zone-center optical phonon replica of the main O^1 transition. Dörnen and Hangleiter (DH) [86D], who reported all three transitions and assigned the O' label, concluded that this system could not be a replica of the O-system due to differences in the lifetimes of corresponding lines, and in the spacing of the lines in the O and O' series. Instead they extended their donor-acceptor-pair model of the O-lines to explain the O' luminescence system by suggesting that these were due to transitions involving some of the singly ionized TDs and residual acceptors. [86D] However, our results

indicate striking similarities between the O- and O'-systems, and we conclude that the IBE-BMEC interpretation can readily explain all of the features of both systems. In this chapter, the spectroscopy of the O'-system is presented in a manner which emphasises the similarities with the O-system described in Chapter 4.

5.2: Experimental Results and Discussion

The sample material used in this PL study of the O′-lines was the same Cz Si as that described in Chapter 3, where the thermal donors were discussed, and in Chapter 4, where the closely related O-system was considered. The O′-system did not appear until after long anneal times: in the 500 °C set of samples it was first observed after 128 h, at which point the PL from the O-system was much stronger. With longer annealing times, PL from the O′-system was found to increase in intensity, as that of the O-system decreased. At very long anneal times, 1024 h at 500 °C, the signal from the O′-system, which was then considerably stronger than that of the O-system, decreased as other luminescence features appeared. The model of DH [86D] does not account for this annealing time dependence of the relative intensities of the O- and O′-systems, since the ratio of neutral to singly-ionized donors should be quite small in these samples, and should not change markedly with annealing time. Furthermore, the long anneal times necessary to generate these systems correlates with the disappearance of the TDs, and not with their creation. We retain the O′ label for this system, but modify the numbering of the lines to reflect the details of our model. The O'_1, O'_2, and O'_3 of DH become, respectively, $O_B^{1\prime}$, $O^{3\prime}$, and $O^{4\prime}$ in our labelling scheme, which exactly parallels the one used for the O-system in the previous chapter.

The many-microsecond scale of the lifetime of $O_B^{1\prime}$ is characteristic of IBE's. Exponential fits to the $O_B^{1\prime}$ decay give lifetimes of 2 μs at 4.2 K and 60 μs at 1.8 K. This increase indicates a split IBE ground state, with

the higher energy $O^{1\prime}_{B}$ component in thermal equilibrium with a dipole-forbidden $O^{1\prime}_{A}$ transition. Such splittings have been observed for other IBE, including the O-center, where luminescence from the O^{1}_{A} transition was detected.[86T] However, no resolved $O^{1\prime}_{A}$ PL could be detected even at the lowest sample temperatures, indicating a more highly forbidden transition, the existence of which can only be inferred from its effect on the $O^{1\prime}_{B}$ lifetime. Much shorter lifetimes are predicted for the BMEC, due to fast Auger processes which are allowed for these complexes, and indeed this is the case. Fitting exponentials to the initial part of the decay curves shown in Figure 5.1 yields lifetimes of 20 ns for $O^{3\prime}$ and 7 ns for $O^{4\prime}$. These did not change with temperature, unlike the $O^{1\prime}_{B}$ lifetime. Note that the time scales used in the figure differ by a factor of 250. The lifetimes of the lines in the O′-system behave in exactly the same manner as the corresponding lines in the O-system, although they are slightly shorter. This is consistent with the fact that the O′-center is more tightly bound. The observation that clearly related PL lines have lifetimes which differ by as much as a factor of 10^{4}, and the temperature dependence of only the $O^{1\prime}_{B}$ line are difficult to explain in the donor-acceptor-pair or free-to-bound recombination model, but are readily predicted by our IBE-BMEC interpretation.

Further support for this interpretation is found in the excitation density dependence of the PL from the O′ system. As shown in Figure 5.2, we observed $O^{1\prime}_{B} > O^{4\prime} > O^{3\prime}$ at high excitation density, $O^{1\prime}_{B} > O^{3\prime} > O^{4\prime}$ at lower levels, followed by the disappearance of $O^{4\prime}$ and then $O^{3\prime}$ at even lower excitation. This behaviour, exactly matching that of the O-system, is once again consistent with $O^{1\prime}$ being a BE, and $O^{3\prime}$ and $O^{4\prime}$ being BMEC

Figure 5.1

PL transient decay curves for the O'-system. Note that the time scale used for (a) and (b) is 250 times shorter than that used for (c). The horizontal markers are decades. (a) and (b) have been arbitrarily shifted from (c). (a) and (b) Fast transient decay curves of $O^{3'}$ and $O^{4'}$ at 1.8 K. Exponential fits to the initial part of the decay curves yield lifetimes of 20 and 7 ns, respectively. (b) has been shifted down one decade for clarity. (c) Decay of the $O^{1'}$ line at 4.2 K, with a lifetime of 2 μs.

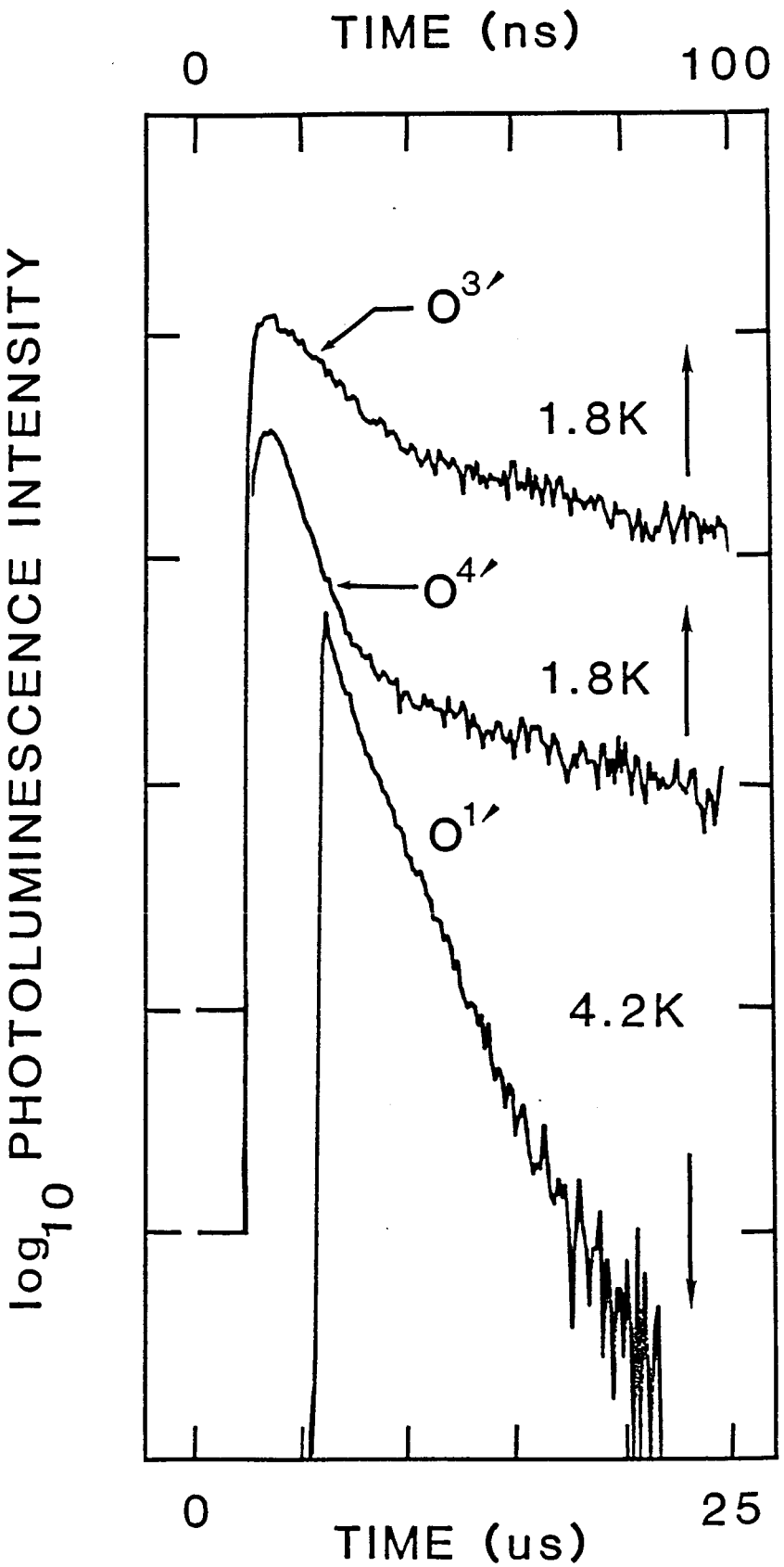
TIME (ns)
0
100
$O^{3'}$
1.8K
$O^{4'}$
1.8K
$O^{1'}$
4.2K
$\log_{10}$ PHOTOLUMINESCENCE INTENSITY
0
25
TIME (us)

Figure 5.2

PL spectra at 1.8 K and three excitation levels from samples annealed at 500°C for 256 h; $I_0 \cong 10$ W/cm^2. All spectra normalized to equal $O^{1\prime}_B$ height.

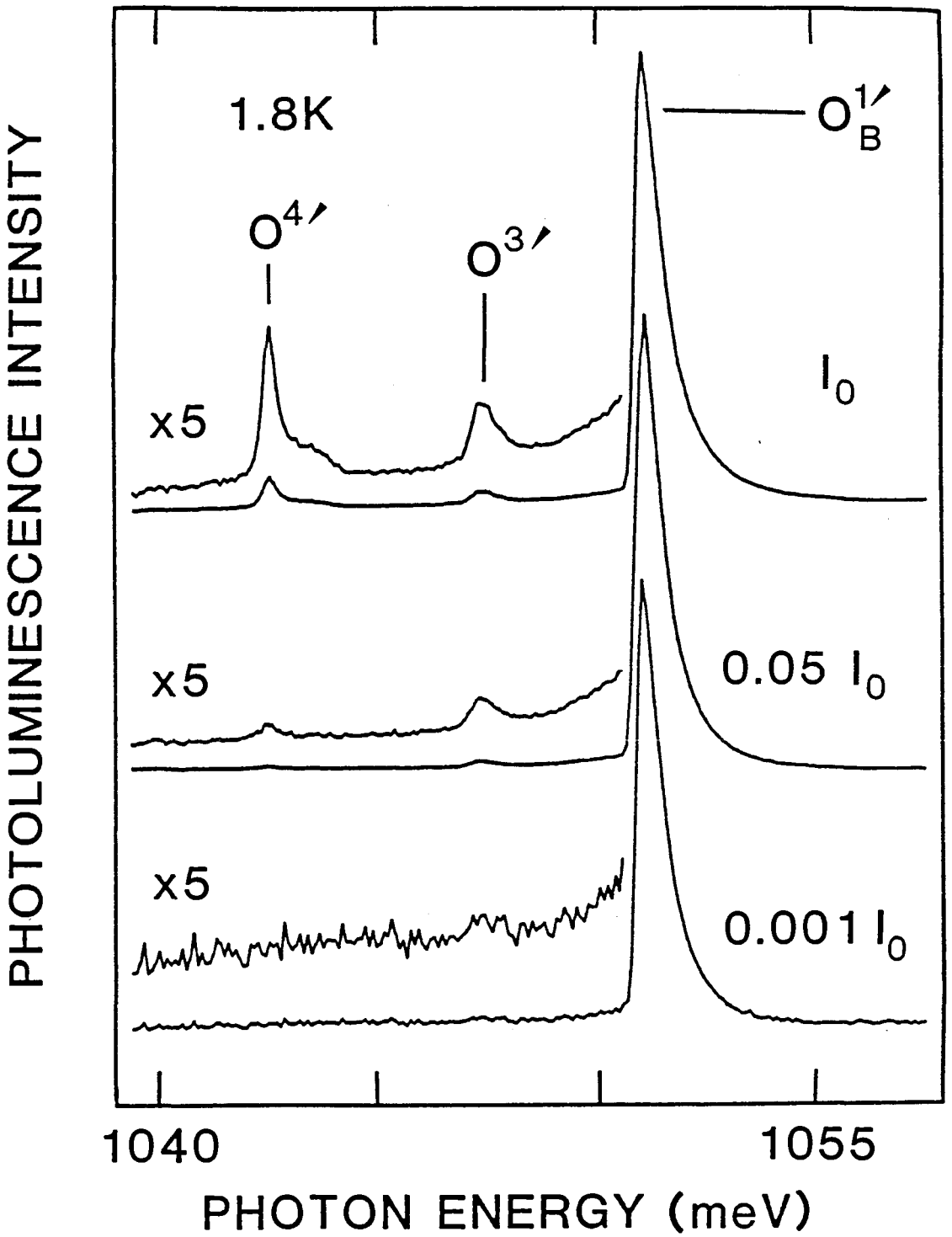
1.8K
$O_B^{1'}$
$O^{4'}$
$O^{3'}$
I_0
x5
x5
0.05 I_0
x5
0.001 I_0
PHOTOLUMINESCENCE INTENSITY
1040
1055
PHOTON ENERGY (meV)

transitions with $O^{4\prime}$ having more *e-h* pairs than $O^{3\prime}$. More systematic measurements of the excitation density dependence of the line intensities revealed that $O^{1\prime}$ has a sublinear dependence, characteristic of BE, while $O^{3\prime}$ and $O^{4\prime}$ are superlinear, typical for BMEC.

The excited state structure of $O^{1\prime}$ as seen in PLE closely resembles that observed for other IBE, particularly O^1. [86T] As shown in Figure 5.3, each state in the O^1 excitation spectrum has a counterpart in the $O^{1\prime}$; our choice of labelling emphasizes this similarity. The spacing of the excited states for these two centers is somewhat different: the ionization limit appears to be about 45 meV above $O^{1\prime}_B$, compared to 30 meV for the O-center. This increase in the binding energy of the weakly bound particle in the IBE with increasing total IBE binding energy is quite typical, and results from the increased localization of the tightly bound particle. The relative intensities and the asymmetric line shapes agree very well between the two spectra.

Just as for the O^1 PLE, the excited states of $O^{1\prime}$ are observed to shift to higher energy when the PL is collected from a narrow band on the high energy tail of the IBE line. This behaviour, indicated in Figure 5.3, confirms that the asymmetric line shape seen in both PL and PLE is due to an inhomogeneous distribution of centers having similar shifts of ground- and excited-state energies, and not due to the kinetic energy of a free particle. Also in agreement with our model is the complete absence of any PLE signal for the $O^{3\prime}$ and $O^{4\prime}$ lines. Since these result from BMEC recombination, their initial states cannot be generated by resonant single photon absorption. None of the other models [86Wa,86Wb,86D] can explain

Figure 5.3

(a) PLE spectum of all $O^{1\prime}$ states, including the $O^{1\prime}$ ground state, with the PL signal detected from the entire broadened $O^{1\prime}_{B}$ line, just as in Figure 9. (b) PLE spectrum with PL pickup in a narrow band 1 meV above the $O^{1\prime}_{B}$ peak. Once again a shift indicating an inhomogeneously broadened distribution is observed. (c) PLE spectrum of all O^{1} states including the O^{1} ground state, shifted in energy so as to align the ground state energies. The similarities in the excited state structure of O^{1} and $O^{1\prime}$ are readily apparent.

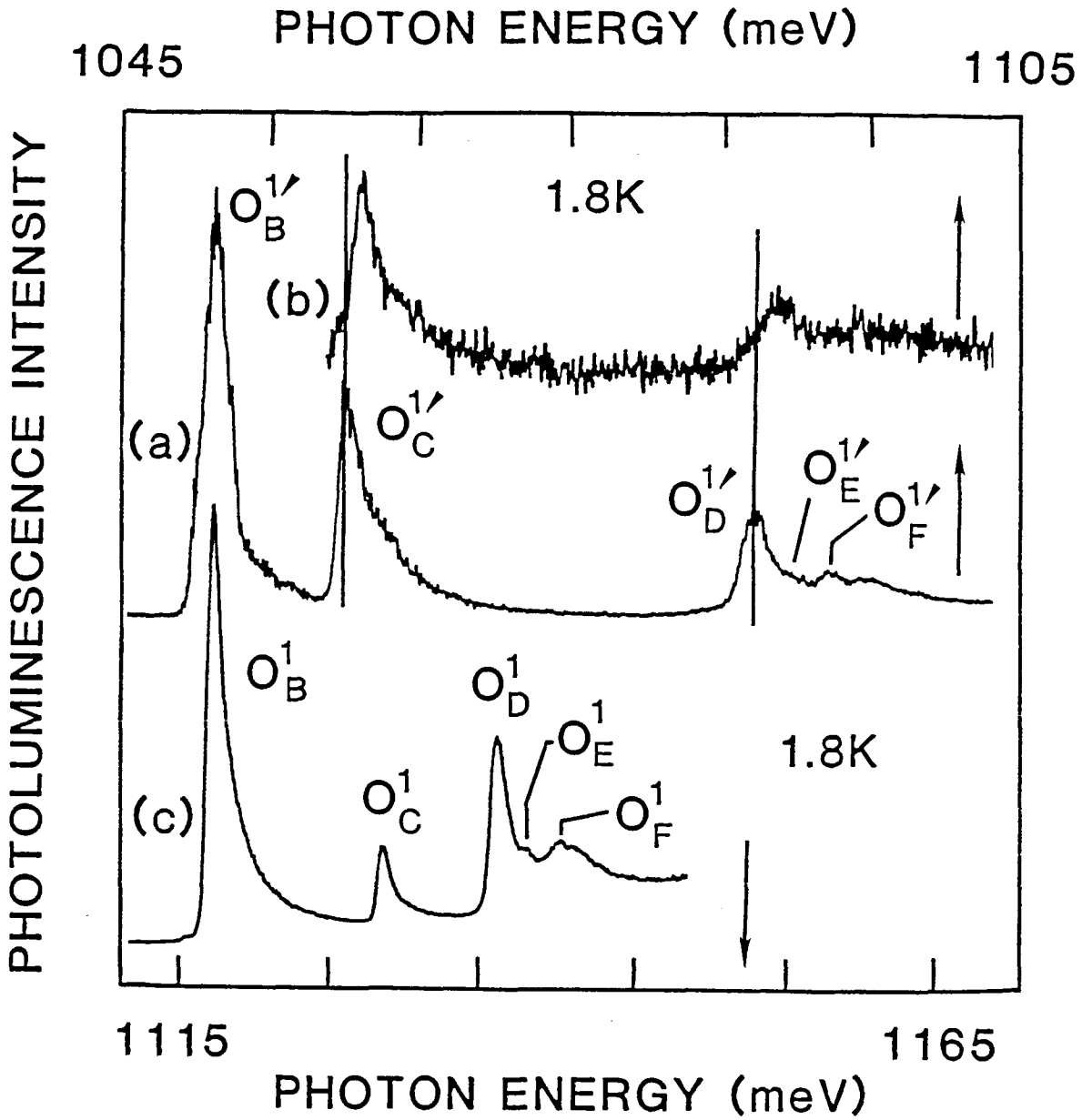
PHOTON ENERGY (meV)
1045
1105
PHOTOLUMINESCENCE INTENSITY
1.8K
(b)
(a)
(c)
1.8K
1115
1165
PHOTON ENERGY (meV)

this striking difference between $O^{1'}$ *versus* $O^{3'}$ and $O^{4'}$ (and O^{1} *versus* O^{3} and O^{4}); neither can they readily explain the IBE-like excited state spectra observed for O^{1} and $O^{1'}$ by PLE.

5.3: Conclusions

The lifetime measurements, excitation-density dependence and PLE spectra provide convincing evidence that the O'-system seen in PL is associated with a BE-BMEC system involving a distribution of very similar isoelectronic centers. The growth of this system with increasing annealing time, which correlates with the decrease in PL from the shallower O-center, suggests that some further chemical reaction, the details of which are as yet unknown, modifies the isoelectronic core which remains after the disappearance of the TDs, and produces the deeper O' isoelectronic center.

CHAPTER 6: DISCOVERY OF POLYEXCITONS

6.1: INTRODUCTION

The analogy between excitons and hydrogenic or positronium systems has been of considerable importance in the development of semiconductor physics and spectroscopy. In 1958, Lampert [58L] used these analogies to predict the existence and properties of a number of new excitonic species, including donor- and acceptor-bound excitons (both neutral and charged), trions (free complexes of two holes and one electron, or *vice versa*), overcharged donors and acceptors (D^- and A^+, respectively), and finally, the (free) excitonic molecule or biexciton.

Wang and Kittel [72W] first pointed out in 1972 that the extra band-edge degeneracy of indirect-gap semiconductors allowed for more novel excitonic systems considerably more complex than those envisioned in the above analogies, since in these semiconductors more than two electrons (namely, twelve for Si and eight for Ge) could be placed into the same ground-state orbital without violating the exclusion principle. Wang and Kittel [72W] were specifically concerned with neutral, free molecular complexes containing more than two electron-hole (*e-h*) pairs, which we shall refer to as polyexcitons (PE). Morgan [77Mb] later gave further theoretical consideration to PE in Si, concluding that PE containing up to at least six *e-h* pairs would be stable.

It is remarkable that no experimental evidence for the existence of these unique excitonic species was obtained in the sixteen years since

their first prediction. This is especially true in light of the large body of experimental evidence regarding bound multiexcitonic complexes (BMECs), which can be thought of as biexcitons or polyexcitons localized on either neutral donors or neutral acceptors. [82T]

In this chapter the first experimental evidence for the existence of free PE, which was obtained from the green photoluminescence (PL) spectrum of highly excited ultrahigh-purity (UHP) Si over a range of sample temperatures, is reported. [87Sa] This process, in which two *e-h* pairs recombine simultaneously to give one photon at almost twice the band-gap energy, has been used previously to study *e-h* plasmas [72Bb] and the "normal" condensed phase of the *e-h* plasma known as the *e-h* droplet (EHD) [72Bc] as well as the biexciton [80S,84T] and BMECs [80S,85Tb] in Si. In addition to being intrinsically very weak, the green PL is also strongly reabsorbed by the Si, necessitating an extremely sensitive detection apparatus. [84T,85Tb]

6.2: Experimental Apparatus and Data Acquisition

Our high-sensitivity PL apparatus was built around an ITT Mepsicron imaging photomultiplier tube with computer-controlled data acquisition, as described in detail by W.G. McMullan.[88M] A block diagram of the experimental setup is shown in Figure 6.1.

Freshly etched samples of UHP Si were mounted in a strain-free manner on the temperature-controlled stage of a VariTemp Dewar. Sample temperatures were measured with a calibrated Si diode and further verified by monitoring of the near-infrared (NIR) free exciton (FE) line shape, which at low temperature has a full width at half maximum proportional to $k_B T$. Excitation was provided by 800 mW of 700 nm laser light from an Ar^+ ion laser-pumped dye laser using LDS 698 dye. This radiation was blocked from the detector by 4 mm of Schott BG39 and BG40 blue pass filters, which had transmission $\cong 10^{-8}$ at 700 nm, and $\cong$ 85% at 540 nm. A 0.75 m Spex 1400 spectrometer equipped with 600 lines/mm gratings used in second order was used to disperse the PL signal. The green luminescence was collected using the Mepsicron tube with typical resolution of $\cong$ 0.5 meV ($\cong$ 0.12 nm). Well-known Ne lines [68S] were used to calibrate the green spectra, and spectral accuracy was to within $\cong$ 0.1 meV in this region. The light-tight compartment surrounding the dewar tail reduced stray light noise to such an extent that the background was essentially dark count limited. The peak intensity of the green polyexciton PL was $\cong$ 4 counts per channel per minute

Figure 6.1

Schematic diagram of the experimental setup for the green photoluminescence spectroscopy of free polyexcitons. By changing the position of the movable mirror in the spectrometer, either the green signal, detected using the Mepsicron imaging photomultiplier tube, or the near infrared signal, detected using the Varian photomultiplier tube, could be monitored without changing the sample position or excitation conditions. (Diagram courtesy of W.G. Mcmullan. [88M])

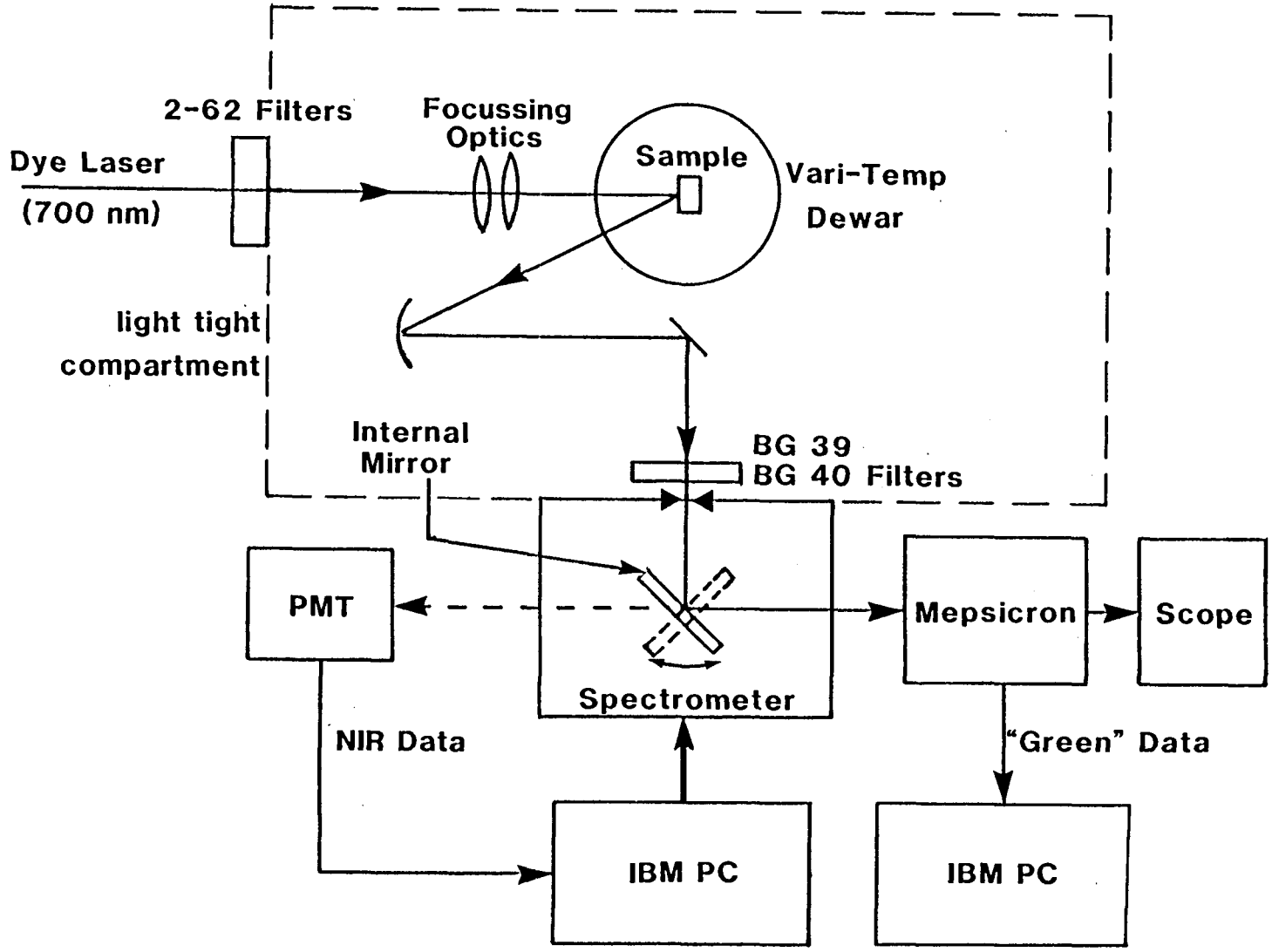
2-62 Filters
Focussing Optics
Dye Laser
(700 nm)
Sample
Vari-Temp Dewar
light tight compartment
Internal Mirror
BG 39
BG 40 Filters
PMT
Mepsicron
Scope
Spectrometer
NIR Data
"Green" Data
IBM PC
IBM PC

(10 times the dark count). Even with this high-sensitivity apparatus, each spectrum required ≅ 20 h to collect.

6.3: Results and Discussion

In Figure 6.2 we summarize the evolution of the green PL spectrum as a function of temperature. Very similar results were obtained in a second UHP Si sample obtained from a different source. The 11 K spectrum is dominated by the broad EHD line, [72Bc,80S,84T,85Tb] which can be quite strong for T < 20 K. A very weak biexciton (X^2) line can also be seen at 11 K, at the same energy as reported previously. [84T]

Upon our increasing the temperature the spectrum changes remarkably, as shown in Figure 6.2. At 20 K, the EHD band is weaker and the X^2 line has grown enormously. This reflects the increase in the equilibrium FE density caused by the reduction of the EHD at temperatures close to the critical temperature for EHD formation, which results in a much larger population of the molecular species. This at first surprising increase of the X^2 population with increasing T was earlier observed by Hulin *et al.* [77Hc] in AgBr. In retrospect, it is unfortunate that prior studies [80S,84T] of the green X^2 luminescence in Si were done at ≅ 2 K, where the signal is extremely weak.

In addition to the intense, sharp X^2 line, the 20 K spectrum reyeals new, resolved structure which we label X^3 and X^4, as well as a shoulder labeled X^5. This same spectrum is shown in more detail in Figure 6.3. We interpret the green X^3 (X^4) line as a transition from a ground-state triexciton (tetraexciton) to a ground-state FE (biexciton). As shown in Figure 6.2, some resolved structure can be observed in the X^2, X^3, X^4 PL up

Figure 6.2

Green photoluminescence of ultrahigh purity Si as a function of temperature, normalized to equal biexciton intensity. The electron-hole droplet band, which dominates the low-temperature spectra, vanishes near 25 K. The biexciton line (X^2) can be observed at all temperatures, while the X^3 - X^5 polyexciton lines appear only at 20 K and above. The calculated lineshape of the "condensed plasma" phase is shown between 20 and 40 K. Its high energy edge is seen to be in poor agreement with that of the observed luminescence. The higher temperature spectra, which were collected for < 20 h, have been shifted to compensate for the reduction of the band gap with increasing T.

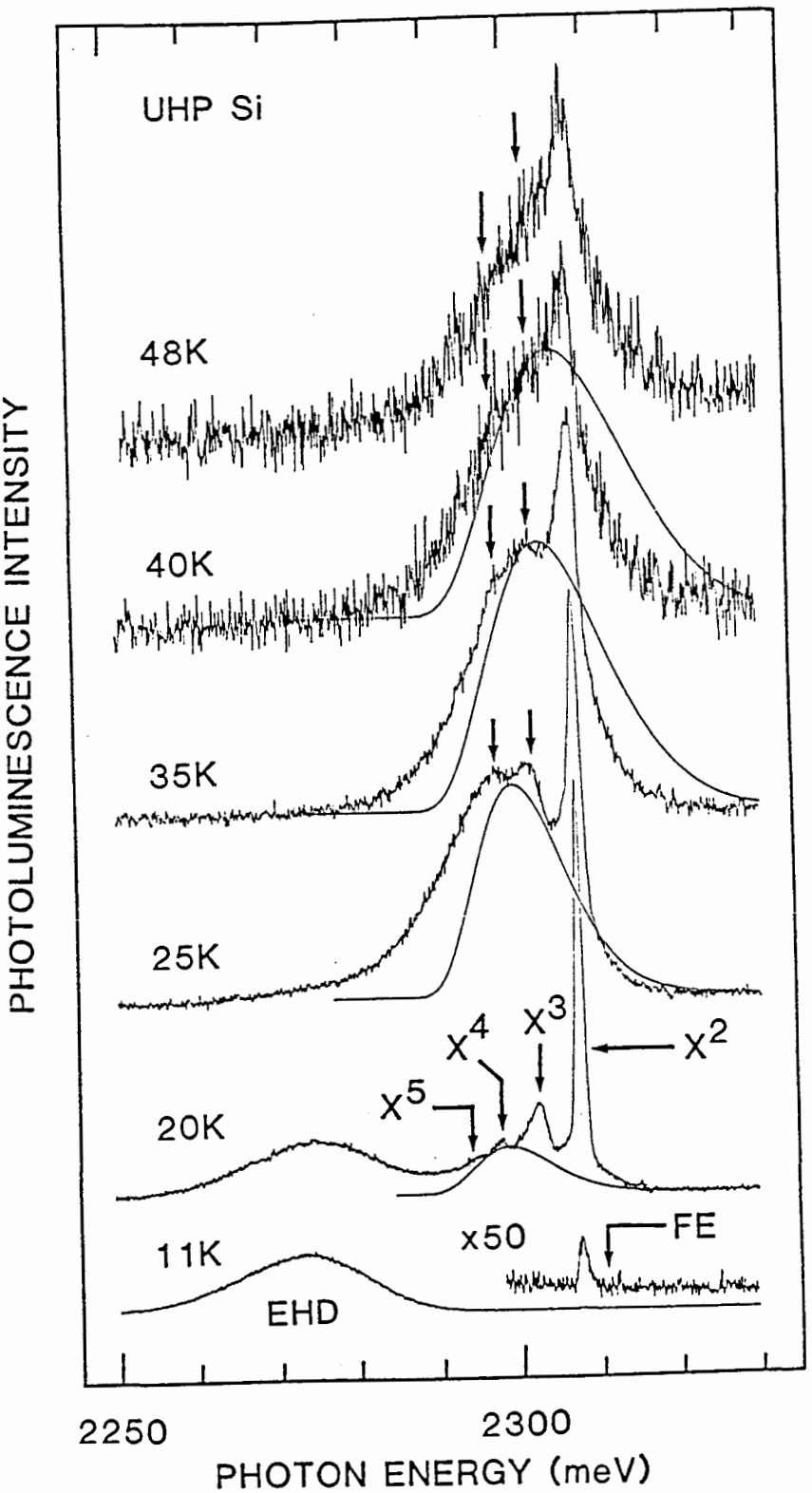
UHP Si
48K
40K
35K
25K
20K
11K
EHD
x50
FE
X2
X3
X4
X5
PHOTOLUMINESCENCE INTENSITY
2250
2300
PHOTON ENERGY (meV)

to at least 40 K. For simplicity we refer only to neutral PE. While charged species larger than X^2 will also be present, their relative concentrations are negligible up to at least 20 K.

Since these lines are observed in two different UHP Si samples, and at temperatures where any localized (bound exciton) states this shallow would be strongly dissociated, an extrinsic explanation can be ruled out. Furthermore, the dependence of X^3-X^5 on FE density is observed to be even more pronounced than that of the biexciton, X^2, as expected for polyexcitons in equilibrium. The strongest support for our PE explanation comes, however, from the luminescence line shapes.

The green process is fundamentally different from the usual NIR PL in two ways. First, since it involves the simultaneous recombination of *two* *e-h* pairs, species such as the FE cannot contribute to the green PL. Second, it is an intrinsic no-phonon process, in which crystal momentum is conserved by having the two recombining electrons in opposite conduction band valleys. The total momentum of the final state must therefore equal the total momentum of the initial state. Since the final state of the X^2 transition is simply the crystal ground state, only biexcitons which are at rest can contribute to the green X^2 PL, resulting in a narrow, symmetrical line. The X^2 line can be broadened by collisions, but not directly by the thermal kinetic energy of the X^2 distribution. [80S,84T]

The situation is more complicated for the PE, since in this case both the initial and final states can have momentum and kinetic energy. When the X^3 decays to a FE, the recoil FE have the same momentum as that of the initial X^3, but since the FE is 3 times lighter it must carry away 3 times

Figure 6.3

The 20 K spectrum of Figure 6.2 on an expanded scale. The solid curve is a fit to the triexciton and tetraexciton lines as described in the text (the amplitude has been expanded by 4 ×). The three vertical arrows mark the transition energies of zero kinetic energy biexcitons, triexcitons, and tetraexcitons, respectively.

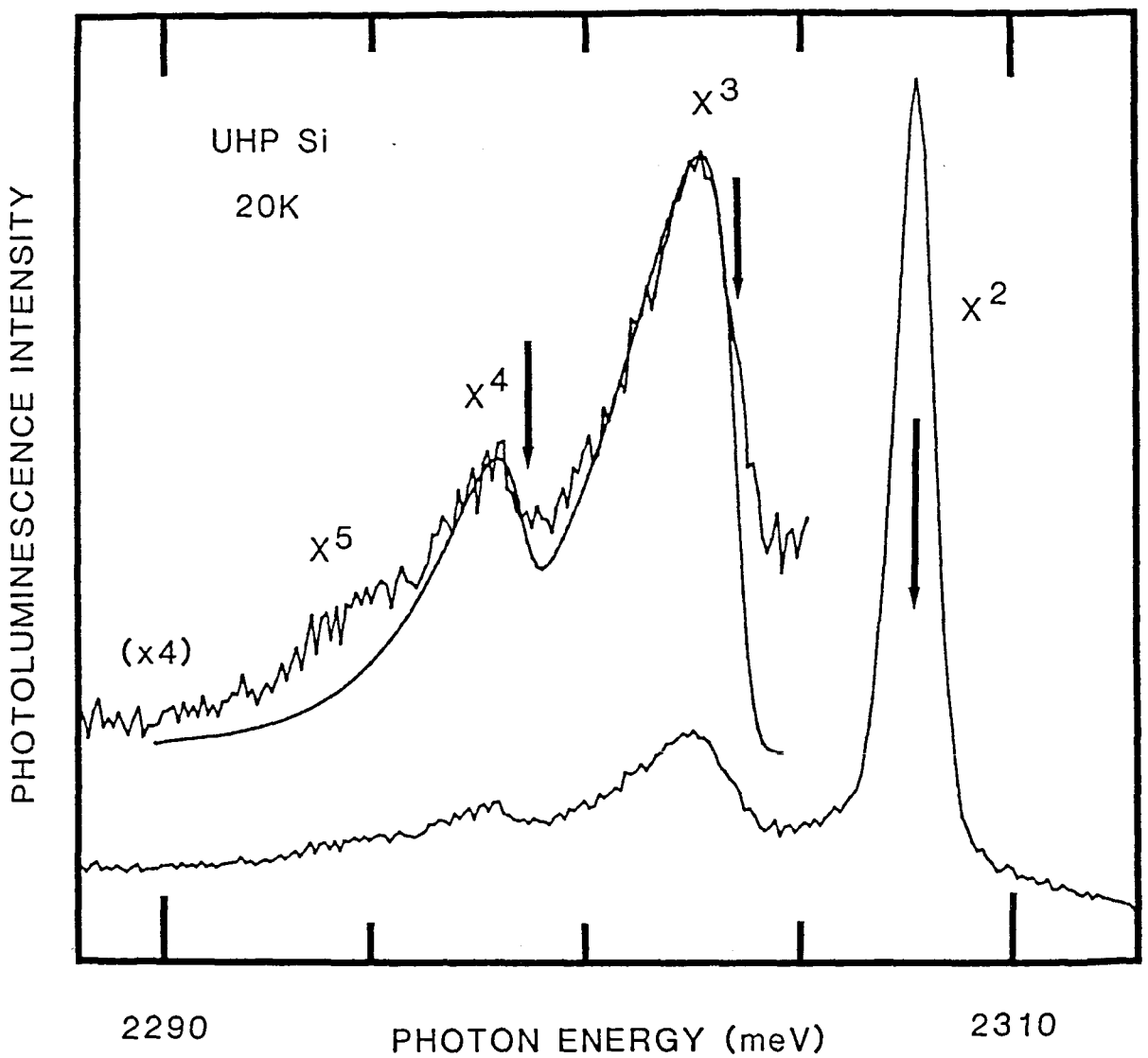
UHP Si
20K
X3
X2
X4
X5
(x4)
PHOTOLUMINESCENCE INTENSITY
2290
PHOTON ENERGY (meV)
2310

the initial kinetic energy. Thus the X^3 PL photon of a triexciton with initial thermal kinetic energy E_k will occur at an energy $2E_k$ *below* that of the recombination of an X^3 at rest. Since the initial polyexciton distribution will be a Maxwell-Boltzmann (with T's very near the lattice temperature), the X^n (n>2) lines should resemble *inverted* Maxwell-Boltzmann line shapes, with thermal tails towards lower energy, as is observed in Figures 6.2 and 6.3.

A more detailed calculation of the PE luminescence line shapes must take into consideration a momentum-dependent matrix element reflecting the overlap of the momenta of the particles in the recoiling final state with those in the initial state. We have adapted a simple model of the NIR biexciton line shape given by Cho [73C] to calculate the green PE line shapes.

In Cho's model, the momentum-dependent matrix element for the biexciton transition X^2 -> FE + $h\nu$ (+ $\hbar\omega_{phonon}$) is given by the sharply peaked function:

$$c(k) = \frac{c_0}{(k^2 + \kappa^2)^2} \qquad \ldots\ldots(6.1)$$

where $\kappa = a_0^{-1}$ is a measure of the biexciton size. Since the recoiling and initial particle wavefunctions must overlap, this imposed cutoff on the allowed momentum spread leads to a low energy cutoff on the reverse Boltzmann line shape observed in PL. This model was used successfully by Thewalt and Rostworowski [77T] to fit the NIR biexciton line shape observed in UHP Si.

For the green luminescence process, it is the sum of the momenta of the recombining particles within the complex which imposes this momentum cutoff. In the picture developed by Cho, this recombination process involves two "excitons" within a PE (with internal wavevectors deviating from the average internal wavevector by k_1 and k_2) which recombine and emit a green photon and leave a recoiling particle with all of the initial momentum. The momentum-dependent matrix element was written as:

$$c(k) = \frac{c_0}{(k_1^2 + \kappa^2)^2 (k_2^2 + \kappa^2)^2} \qquad \ldots\ldots (6.2)$$

Using a quadratic dispersion relation $\varepsilon = \frac{\hbar k^2}{2m}$ to change the momentum integral obtained from this extension of Cho's model into an energy integral, the cutoff equation becomes:

$$c(E) = c_0 \int_0^\infty d\varepsilon \, \frac{\varepsilon^2}{(\varepsilon + \Gamma_j)^2} \left(((\varepsilon^{1/2} + \tfrac{2}{3} E^{1/2})^2 + \Gamma_j^2) \; ((\varepsilon^{1/2} - \tfrac{2}{3} E^{1/2})^2 + \Gamma_j^2) \right)^{-1} \qquad \ldots\ldots (6.3)$$

Here Γ_j is Cho's parameter κ in energy units, which is an adjustable parameter, used to change the width of the distribution.

Finally, the luminescence line shape in the green may be obtained from this transition matrix element using Fermi's Golden Rule, just as for the NIR PL. [77T] The resulting expression is:

$$I(E) = \sqrt{E_x - \tfrac{1}{2}(E + E_{jb})} \cdot \exp\left(\frac{\sqrt{E_x - \frac{1}{2}(E + E_{jb})}}{k_B T} \right) \cdot \left| c(E) \right|^2 \qquad \ldots\ldots (6.4)$$

In Equation 6.4, the luminescence photon energy is E, while E_x is the energy at which a zero kinetic energy FE transition would appear if this process were allowed, and E_{jb} is the energy of the zero kinetic energy transition from the jth PE, which determines the binding energy. The binding energy, E_{jb} is also an adjustable parameter, which determines the high energy onset of the distribution, corresponding to transitions from stationary PE.

The best-fit results are shown in Figure 6.3, where T was taken as the lattice temperature, and the zero-kinetic-energy transition energies (arrows) and the line width parameters Γ_j [73C] were optimized. The resultant binding energies, defined in terms of removal of one FE ($X^j \rightarrow X^{j-1} + FE$), were 1.36, 3.83, and 6.34 meV for X^2, X^3, and X^4, respectively. There are as yet no reliable theoretical estimates of the PE binding energies for comparison. The "radii", as determined from the Γ_j, were 100 and 130 Å for X^3 and X^4, as compared to 100 Å obtained earlier [77T] for X^2, but these should not be taken rigorously, considering the approximations contained in the theory. [73C]

The binding energy of the pentaexciton (X^5) cannot be obtained from the observed X^5 line, since in analogy to the shell model [77Ka,77Kb] used to describe BMECs [82T] X^5 must have holes in two different shells (the valence-band edge is only fourfold degenerate). Thus the lowest energy X^5 transition, which is the one observed by us, leaves the final X^3 in an electronic excited state (two holes in the ground shell, one in the upper shell). Just as for BMECs, [80Tc,82T] there must be a second (weaker) X^5 ground-state to ground-state transition, but it is hidden under the stronger X^2 - X^4 lines.

Smith and Wolfe (SW) [86Sa,86Sb,88Sa] have recently interpreted a band seen in time-resolved NIR PL of UHP Si as a new (and unexpected) condensed phase of the *e-h* plasma (CP), having a density ≅ 10 times lower than that of the EHD, and a critical temperature of ≅ 45 K. It was the extra luminescence band attributed in Figure 6.4 to polyexcitons which SW interpreted as being due to the CP. They fit theoretical line shapes to the FE, EHD, and biexciton components, subtracted them from the experimental data, and then fit a plasma line shape to the remaining signal. The observed independence of the line shape of this band on the FE density was the basis for concluding that a second condensed phase existed. Hernandez [87H] has recently questioned the CP model, and proposed that the band may originate from excitonic complexes.

This alternative explanation is made more compelling by our discovery of the existence of PE, which are seen to have quite large binding energies and to be present in considerable quantities in the same T and FE-density regimes where the "CP" band is observed. The PE observed by us in the green PL would have a broad, unresolved, NIR PL line shape very similar to that of the CP band of SW. [86Sa,86Sb,88Sa] The NIR polyexciton line shapes are determined only by T and the momentum matrix elements, and although some dependence of the relative intensities of transitions from different PE initial states on the time-varying FE density is expected, the widths of the lines would obscure any such changes on the scale of the very weak, ill-resolved PL signal observed in this region. We have observed the "CP" band in the NIR PL of our samples under exactly the same conditions which produce resolved PE structure in the green PL. The TO phonon replica PL spectrum collected at approximately 25 K and shown in Figure 6.4

illustrates the nature of the "ordinary" luminescence in this region. The large FE signal completely dominates the spectrum, and while it is possible to observe the biexciton, no further resolved structure in the excitonic region may be seen. The EHD seen even at this temperature indicates a large FE density due to our excitation conditions.

Furthermore, the green PL shows little evidence of a CP component, the expected line shape of which has been indicated on the 20 - 40 K spectra of Figure 6.2. Of course this does not prove that the CP does not exist, since one could argue either that its green PL is very weak, or that it does not exist near enough to the surface to be observed under our experimental conditions.

Nevertheless, since we have demonstrated that the PE exist, they must surely contribute some intensity to the NIR CP band. The question then is whether the near-infrared polyexciton PL can account for the entire CP band. SW [86Sb,88Sa] have argued that it cannot, on the basis of thermodynamic calculations of the populations of the various species. However, their calculations [86Sb,88Sa] were based upon a uniform *average* FE density, which is not a good description of the spatial distributions present in their experiments. The use of an average FE density, rather than the true spatially varying distribution, can lead to a serious underestimate of the net concentration of the larger complexes, which are strongly enhanced by small increases in the FE density.

Figure 6.4

Near infrared spectrum of the intrinsic luminescence in the transverse optical phonon assisted region near 25 K. The principal feature is the free exciton transiton, with the biexciton and unresolved polyexciton transitions at lower energy. A small luminescence component due to recombination within the electron-hole droplet is also indicated in the figure.

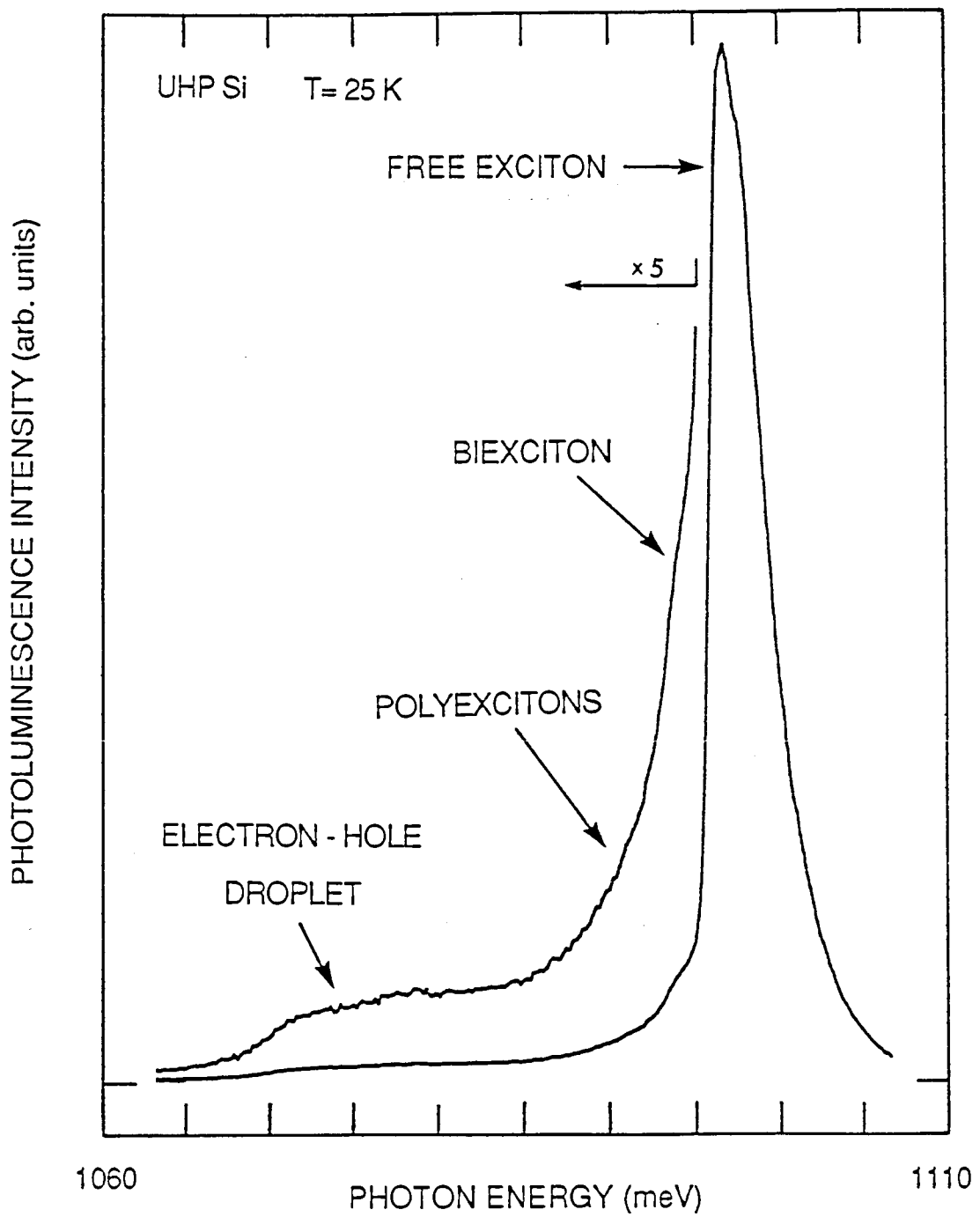
UHP Si T= 25 K
FREE EXCITON
x 5
BIEXCITON
POLYEXCITONS
ELECTRON - HOLE
DROPLET
PHOTOLUMINESCENCE INTENSITY (arb. units)
1060
1110
PHOTON ENERGY (meV)

We have applied the same Richardson-type equations used by SW [88Sa] to a radially decaying, hemispherically symmetric FE distribution, which is a more accurate description of the true experimental [86Sb,88Sa] situation. The spatial density profile of each excitonic species about the excitation spot at the crystal surface was taken to be a Gaussian of the form:

$$n_j(r) = n_{j0} \exp\left(\frac{-jr^2}{r_0^2} \right) \qquad (j = 1 \text{ to } 4)$$

.....(6.5)

The Richardson-type equations [86Sb,88Sa] for the concentrations of each excitonic species depend on the temperature, T, and chemical potential, μ, of the gas, as well as the degeneracy g_j, dissociation energy Δ_j, and mass m_j of each:

$$n_j = g_j \left(\frac{m_j kT}{2\pi\hbar^2} \right)^{3/2} \exp\left(\frac{(j\mu + \Delta_j)}{kT} \right)$$

.....(6.6)

The translational mass of the FE is $m_{FE} = 1.22 \cdot m_e$ [77L], and the larger complexes were taken to have $m_j = j \cdot m_{FE}$. The degeneracies, obtained by considering the 12-fold degenerate conduction band minimum and the 4-fold degenerate valence band maximum, and the total dissociation energies required to break each complex into j FE are listed in Table 6.1 below for the first four neutral excitonic complexes. Once the ratio of the biexciton density to the FE density is obtained from the experimental data, the chemical potential μ which appears in the exponential of Equation 6.6 can be determined. Since μ is the only unknown quantity in Equation 6.6, the density of each polyexcitonic species may then be calculated directly. In

j	g_j	Δ_j (meV)
1	48	0
2	396	1.36
3	880	5.19
4	495	11.53

Table 6.1: Degeneracy factor, g_j, and total dissociation energy, Δ_j, for neutral excitonic species containing j *e-h* pairs.

particular, the ratios of the triexciton and tetraexciton densities to the biexciton density, and hence the ratios of the total numbers of these species to the total number of biexcitons within the hemispherical density profile model described by Equation 6.5 can be calculated. No free parameters enter into this analysis, once the biexciton to FE ratio has been obtained, and this procedure is described below.

The luminescence intensity of each species is proportional to the total number divided by the luminescence lifetime of each: $I_j \propto N_j/\tau_j$. To estimate the relative lifetimes, the B BMEC lifetimes were plotted *versus* number of bound particles, [82T] and then the interpolated lifetimes for 2, 4, 6, and 8 particles were used for the FE, bi-, tri-, and tetraexctions, respectively. Because of the very small boron central cell potential, this was expected to give a reasonable approximation. The lifetimes obtained, with τ_{FE} normalized to unity, were: 0.326, 0.171, and 0.108 for X^2, X^3, and X^4.

In the Gaussian-profile model, the total number of each species is obtained from the integral:

$$N_j = \int_\tau n_j(r)\, dV \qquad (j = 1 \text{ to } 4)$$

$$= \pi\, n_{j0} \int_0^\infty r^2 \exp\left(-jr^2 / r_0^2 \right) dr$$

$$= n_{j0} \left(\frac{\pi r_0^2}{2\, j} \right)^{3/2} \qquad \ldots\ldots (6.7)$$

The FE density at the origin of this distribution was then adjusted so that the calculated X^2 to FE PL ratio matched that observed by SW. [86Sb] From their data at 20.3 K, the PL peak intensity ratio $I(X^2)/I(FE) = 0.27$. From this ratio, all of the densities n_{j0} are determined and there are no adjustable parameters in the calculation.

The observed ratio of the CP luminescence to the biexciton luminescence was $I(CP)/I(X^2) = 0.72$. [86Sb] Under the conditions discussed above, the calculated total relative PE PL intensity was in fact very close to that of the observed [86Sb] CP band: $\left(I(X^3) + I(X^4)\right)/I(X^2) = 0.75$. This lends credence to the claim that the extra NIR luminescence in Figure 6.4 not accounted for by the FE and biexciton transitions is accounted for by the NIR transitions of PE. Of course, this still does not prove that no CP exists, or that the only PL in the extra band is due to PE.

Smith and Wolfe have also attempted to explain part of our green PL results by fitting a plasma line shape to the low energy edge of our 35 K PL spectrum [88Sb] and concluded that more than half of the total PL intensity in this region is due to a high density plasma with an average density of 6×10^{17} cm^{-3}. While we agree that our green PL spectra will contain some *e-h* plasma component, their fit [88Sb] seems improbable. As with the expected line shape of the CP in the green shown in Figure 6.2, their higher density plasma line shape has a long tail to high energy which is still too large to properly describe the high energy edge of the observed spectrum. In particular, the biexciton line shape derived from their fit is quite unlikely to be correct. Once again, however, we should point out that a high density *e-h* plasma, FE, biexcitons, and both neutral and ionized PE are all to be expected under our excitation conditions, and

consequently extreme care must be taken when any fit to such a complicated spectrum is attempted.

In order to illustrate the danger of attempting to force a fit using an incomplete picture of the various processes which contribute to the observed PL spectra, we have fit the biexciton region using a Lorentzian distribution, which is the expected line shape of a collision-broadened transition. By increasing the full width at half maximum of the Lorentzian to 3.8 meV, it was possible to fit adequately the entire high-energy portion of the same 35 K spectrum with the biexciton line shape alone, as shown in Figure 6.5. While we are not suggesting that this simple single-component fit to the data necessarily represents a complete description of the PL in the high energy region, when compared to the result of SW,[88Sb] our figure adequately demonstrates that various good fits to one portion of the spectrum can be made by emphasizing a single decay channel at the expense of all others. It is apparent that a careful and complete analysis of *all* components in the spectrum is required, which may not be unambiguously possible given the limited information available.

Figure 6.5

Lorentzian fit to the biexciton region in the green photoluminescence spectrum collected at 35 K. While we are not suggesting that this necessarily represents a physically realistic description of all of the luminescence in this region, it is clear that the high energy edge of the spectrum can be fit adequately by considering only collision broadening. This fit illustrates the possible danger in attempting to force a fit to one region of the spectrum without regard for other decay processes.

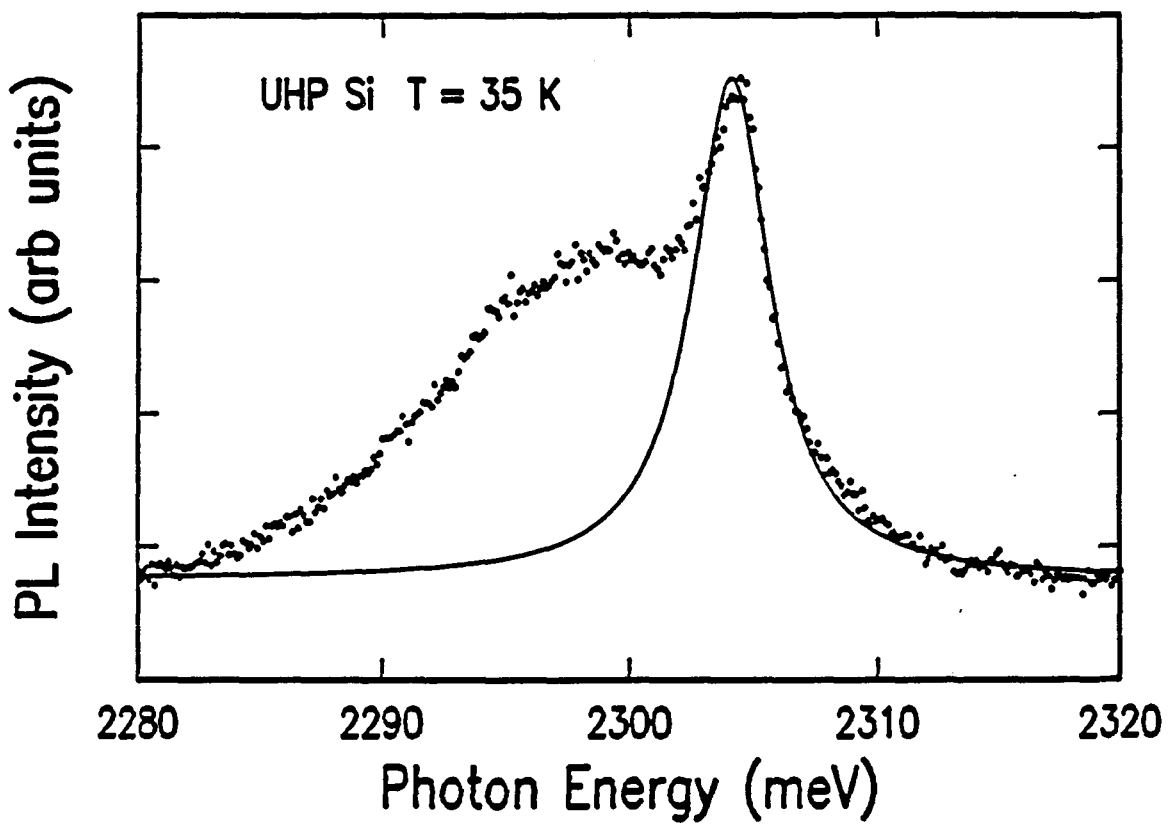
UHP Si T = 35 K
PL Intensity (arb units)
2280
2290
2300
2310
2320
Photon Energy (meV)

6.4: Conclusions

This chapter has reported the first observation of free polyexcitons in a semiconductor, and measured the binding energy of triexcitons and tetraexcitons in Si. Line shape analysis based on a simple transition matrix element adapted from Cho [73C] was used to obtain these binding energies. In addition, it has been demonstrated that polyexcitons can provide an alternative explanation for the new "condensed plasma" phase reported by Smith and Wolfe, [86Sa,86Sb,88Sa] since the expected NIR polyexciton luminescence intensity obtained from thermodynamic arguments is large enough to account for the observed signal.

REFERENCES

31F Frenkel, J., Phys. Rev. **37**, 1276 (1931).

37W Wannier, G.H., Phys. Rev. **52**, 191 (1937).

54F Fuller, C.S., J.W. Dietzenberger, N.B. Hannay, and E. Buehler, Phys. Rev. **96**, 833 (1954).

57F Fuller, C.S. and R.A. Logan, J. Appl. Phys. **28**, 1427 (1957).

57K Kaiser, W., Phys. Rev. **105**, 1751 (1957).

58H Hrostowsky, H.J., and R.H. Kaiser, Phys. Rev. Lett. **1**, 199 (1958).

58K Kaiser, W., H.L. Frisch, and H. Reiss, Phys. Rev. **112**, 1546 (1958).

58L Lampert, M.A., Phys. Rev. Lett. **1**, 450 (1958).

60H Haynes, J.R., Phys. Rev. Lett. **4**, 361 (1960).

62L Long, D., J. Appl. Phys. **33**, 1682 (1962).

65H Hensel, J.C., H. Hasegawa, and M. Nakayama, Phys. Rev. Lett. **138**, A225 (1965).

65K Kohn, W., Solid State Physics **5**, 257 (1965).

66Ha Haynes, J.R., Phys. Rev. Lett. **17**, 860 (1966).

66Hb Hopfield, J.J., D.G. Thomas, and R.T. Lynch, Phys. Rev. Lett. **17**, 312 (1966).

67C Cuthbert, J.D., and D.G. Thomas, Phys. Rev. **154**, 763 (1967).

68A Asnin, V.M., and A.A. Rogachev, JETP Lett. **7**, 360 (1968).

68K Keldysh, L.V., in *Proceedings of the Ninth International Conference on the Physics of Semiconductors, Moscow 1968*, edited by S.M. Ryvkin (Nauka, Leningrad, 1968), p. 1303.

68S Striganov, A.R., and N.S. Sventitskii *Tables of Spectral Lines of Neutral and Ionized Atoms* (IFI/Plenum, New York-Washington, 1968).

69M Merz, J.L., R.A. Faulkner, and P.J. Dean, Phys. Rev. **188**, 1228 (1969).

70K Kaminskii, A.S., and Ya. E. Pokrovskii, JETP Lett **11**, 255 (1970).

70S Shaklee, K.L., and R.E. Nahory, Phys. Rev. Lett. **24**, 942 (1970).

71A Allen, J.W., J. Phys. C **4**, 1936 (1971).

72Ba Bean, A.R., and R.C. Newman, J. Phys. Chem. Solids **33**, 255 (1972).

72Bb Betzler, K., T. Weller, and R. Conradt, Phys. Rev. **B6**, 1394 (1972).

72Bc Betzler, K., and R. Conradt, Phys. Rev. Lett. **28**, 1562 (1972).

72N Nilsson, G., and G. Nelin, Phys. Rev. **B6**, 3777 (1972).

72W Wang, J., and C. Kittel, Physics Lett. **42A**, 189 (1972).

73B Brinkman, W.F., and T.M. Rice, Phys. Rev. **B7**, 1508 (1973).

73C Cho, K., Opt. Commun. **8**, 412 (1973).

73G Graff, K., E. Grallath, S. Ades, G. Goldbach, and J. Toelg, Solid State Electr. **16**, 887 (1973).

75G Graff, K., and H. Pieper, J. Electron. Mater. **4**, 281 (1975).

76B Baldereschi, A., and N.O. Lipari, in *Proceedings of the Thirteenth International Conference on the Physics of Semicondors, Rome 1976* (Rome, 1976) pp. 595-598.

76P Pelant, I., A. Mysyrowicz, and C. Benoît à la Guillaume, Phys. Rev. Lett. **37**, 1708 (1976).

76S Schmid, W., Solid State Commun. **19**, 347 (1976).

77Ha Helmreich, O., and E. Sirtl, in *Semiconductor Silicon 1977*, edited by R.H. Huff and E. Sirtl, (The Electrochemical Society, Princeton, 1977) p. 626.

77Hb Hensel, J.C., T.G. Phillips, and G.A. Thomas, Solid State Physics **32**, 88 (1977).

77Hc Hulin, D., A. Mysyrowicz, M. Combescot, I. Pelant, and C. Benoît à la Guillaume, Phys. Rev. Lett. **39**, 1169 (1977).

77Ka Kirczenow, G., Solid State Commun. **21**, 713 (1977).

77Kb Kirczenow, G., Can. J. Phys. **55**, 1787 (1977).

77L Lipari, N.O., and M. Altarelli, Phys. Rev. **15**, 4883 (1977).

77Ma Martin, R.W., and H.L. Störmer, Solid State Commun. **22**, 523 (1977).

77Mb Morgan, T.N., Nuovo Cimento Soc. Ital. Fis. B **39**, 602 (1977).

77R Rice, T.M., Solid State Physics **32**, 1 (1977).

77S Schmid, W., Physica Status Sol. (b) **84**, 529 (1977).

77T Thewalt, M.L.W., and J.A. Rostworowski, Solid State Commun. **25**, 991 (1977).

77V Vouk, M.A., and E.C. Lightowlers, J. Phys. C **10**, 3689 (1977).

78M Muller, S.H., M. Sprenger, E.G. Sieverts, and C.A.J. Ammerlaan, Solid State Commun. **25**, 987 (1978).

78Ta Tajima, M., Appl. Phys. Lett. **32**, 719 (1978).

78Tb Timusk, T., H. Navarro, N.O. Lipari, and M. Altarelli, Solid State Commun. **25**, 217 (1978).

79D Dean, P.J., and D.C. Herbert, in *Topics in Current Physics* **14**, edited by K. Cho (Springer, Berlin, Heidelberg, 1979).

79G Gaworzewski, P., and K. Schmalz, Phys. Status Solidi (a) **55**, 699 (1979),

79S Schmid, W., Physica Status Sol. (b) **94**, 413 (1979).

79Ta Tajima, M., A. Kanamori, and T. Iizuka, Jap. J. Appl. Phys **18**, 1401 (1979).

79Tb Thewalt, M.L.W., J.A. Rostworowski, and G. Kirczenow, Can. J. Phys. **57**, 1898 (1979).

79Wa Weber, J., W. Schmid, and R. Sauer, J. Lumin. **18/19**, 93 (1979).

79Wb Wruck, D. and P. Gaworzewski, Phys. Status Solidi (a) **56**, 557 (1979).

80H Hammond, R.B., and R.N. Silver, Appl. Phys. Lett. **36**, 68 (1980).

80S Schmid, W., Phys. Rev. Lett. **45**, 1726 (1980).

80Ta Tajima, M., S. Kishino, M. Kanamori, and T. Iizuka, J. Appl. Phys. **51**, 2247 (1980).

80Tb Tajima, M., A. Kanamori, S. Kishino, and T. Iizuka, Jap. J. Appl. Phys **19**, L755 (1980).

80Tc Thewalt, M.L.W., J. Phys. Soc. Jpn. **49A**, 437 (1980).

81G Gourley, P.L., and J.P. Wolfe, Phys. Rev. **B24**, 5970 (1981).

81K Kimmerling, L.C., and J.L. Benton, Appl. Phys. Lett. **39**, 410 (1981).

81M Minaev, N.S., and A.V. Mudryi, Phys. Status. Solidi (a) **68**, 561 (1981).

81T Tajima, M., T. Masui, T. Abe, and T. Iizuka, in *Semiconductor Silicon 1981*, edited by H.R. Huff, R.J. Kriegler, and Y. Takeishi (Electrochem. Soc., Pennington, 1981) p. 72.

82G Gourley, P.L., and J.P. Wolfe, Phys. Rev. **B25**, 6338 (1982).

82T Thewalt, M.L.W. in *Excitons*, edited by E.I. Rashba and M.D. Sturge (North-Holland, New York, 1982), pp. 394-458.

83Oa Oeder, R., and P. Wagner, in *Defects in Semiconductors II*, edited by S. Mahajan and J.W. Corbett (North-Holland, New York, 1983), p. 171.

83Ob Oehrlein, G.S., J. Appl. Phys. **54**, 5453 (1983).

83P Pajot, B., H. Compain, J. Leroneille, and B. Clerjaud, Physica (Utrecht) **117B**, 110 (1983).

83S Stavola, M., J.R. Patel, L.C. Kimmerling, and P.E. Freeland, Appl. Phys. Lett. **42**, 73 (1983).

84C Corbett, J.W., H.L. Frisch, and L.C. Snyder, Mater. Lett. **2**, 209 (1984).

84D Davies, G., J. Phys. C: Solid State Phys. **17**, 6331 (1984).

84O Ourmazd, A., W. Schröter, and A. bourret, J. Appl. Phys. **56**, 1670 (1984).

84S Steiner, T., and M.L.W. Thewalt, Solid State Commun. **49**, 1121 (1984).

84T Thewalt, M.L.W., and W.G. McMullan, Phys. Rev. **B30**, 6232 (1984).

84W Watkins, S.P., M.L.W. Thewalt, and T. Steiner, Phys. Rev. **B29**, 5727 (1984).

85N Newman, R.C., J. Phys. C: Solid State Phys. **18**, L967 (1985).

85S Stavola, M., K.M. Lee, J.C. Nabity, P.E. Freeland, and L.C. Kimmerling,, Phys. Rev. Lett. **54**, 2639 (1985).

85Ta Thewalt, M.L.W., D. Labrie, and T. Timusk, Solid State Commun. **53**, 1049 (1985).

85Tb Thewalt, M.L.W., and W.G. McMullan in *Proceedings of the Seventeenth International Conference on the Physics of Semiconductors*, edited by J.D. Chadi and W.A. Harrison (Springer-Verlag, New York, 1985), p. 1243.

86D Dörnen, A., and A. Hangleiter in *Defects in Semiconductors III*, edited by H.J. von Bardeleben (Materials Science Forum, Switzerland, 1986) p. 967.

86G Griffin, J.A., H. Navarro, and L. Genzel, in *Oxygen, Carbon, Hydrogen and Nitrogen in Crystalline Silicon*, edited by J.W. Corbett, J.C. Mikkelsen, Jr., S.J. Pearton, and S.J. Pennycook (Materials Research Society, Pittsburgh, 1986).

86M Michel, J., J.R. Niklas, J.-M. Spaeth, and C. Weinert, Phys. Rev. Lett. **57**, 611 (1986).

86Sa Smith, L.M., and J.P. Wolfe, Phys. Rev. Lett. **57**, 2314 (1986).

86Sb Smith, L.M., and J.P. Wolfe, Phys. Rev. Lett. **58**, 2823 (1986).

86Sc Steiner, T., PhD. Thesis, Simon Fraser University (1986).

86T Thewalt, M.L.W., A.G. Steele, S.P. Watkins, and E.C. Lightowlers, Phys. Rev. Lett. **57**, 1939 (1986).

86Wa Weber, J., and H.J. Queisser, in *Oxygen, Carbon, Hydrogen and Nitrogen in Crystalline Silicon*, edited by J.W. Corbett, J.C. Mikkelsen, Jr., S.J. Pearton, and S.J. Pennycook (Materials Research Society, Pittsburgh, 1986).

86Wb Weber, J., K. Köhler, F.J. Stützler, and H.J. Queisser in *Defects in Semiconductors III*, edited by H.J. von Bardeleben (Materials Science Forum, Switzerland, 1986) p. 979.

86Wc Watkins, S.P., PhD. Thesis, Simon Fraser University (1986).

87G Gregorkiewicz, T., D.A. van Wezep, H.H.P. Th. Bekman, and C.A.J. Ammerlaan, Phys. Rev. **B35**, 3810 (1987).

87H Hernandez, J.P., Phys. Rev. Lett. **58**, 2822 (1987).

87Ma McL Colley, P., and E.C. Lightowlers, Semicond. Sci. Technol. **2**, 157 (1987).

87Mb Monemar, B., U. Lindefelt, and W.M. Chen, Physica **146B**, 256 (1987).

87Sa Steele, A.G., W.G. McMullan, and M.L.W. Thewalt, Phys. Rev. Lett. **59**, 2899 (1987).

87Sb Steele, A.G., M.L.W. Thewalt, and S.P. Watkins, Solid State Commun. **63**, 81 (1987).

88B Bekman, H.H.P. Th., T. Gregorkiewicz, and C.A.J. Ammerlaan, Phys. Rev. Lett **61**, 227 (1988).

88C Charbonneau, S., PhD. Thesis, Simon Fraser University (1988).

88Da Davies, G., to be published in Physics Reports (1988).

88Db Drakeford, A.C.T., and E.C. Lightowlers in Mat. Res. Soc. Symp. Proc. Vol. 104, pp. 209-213 (1988).

88L Labrie, D., M.L.W. Thewalt, I.J. Booth, and G. Kirczenow, Phys. Rev. Lett. **61**, 1882 (1988).

88M McMullan, W.G., PhD. Thesis, Simon Fraser University (1988).

88Sa Smith, L.M., PhD. Thesis, University of Illinois at Urbana Champagne (1988).

88Sb Smith, L.M., and J.P. Wolfe, Private Communication (to appear as a Comment in Phys. Rev. Lett.) (1988).

88T Thewalt, M.L.W., D.J. Beckett, and M.N. Nissen, presented as an Invited Paper at *The Third International Conference on Shallow Defects in Semiconductors* (Linköping, Sweden, August 1988) (proceedings to be published in the I.O.P. Conference Series).